

Combining Physics-based and Data-driven Modeling for Building Energy Systems

Leandro Von Krannichfeldt^{a,b,*}, Kristina Orehounig^{b,c} and Olga Fink^a

^aEPFL, Route Cantonale, Lausanne, 1015, Switzerland

^bSwiss Federal Laboratories for Materials Science and Technology (Empa), Überlandstrasse 126, Dübendorf, 8600, Switzerland

^cVienna University of Technology (TUW), Karlsplatz 13, Vienna, 1040, Austria

ARTICLE INFO

Keywords:

Building Energy Modeling
Hybrid Modeling
Temperature Prediction

Abstract

Building energy modeling plays a vital role in optimizing the operation of building energy systems by providing accurate predictions of the building's real-world conditions. In this context, various techniques have been explored, ranging from traditional physics-based models to data-driven models. Recently, researchers are combining physics-based and data-driven models into hybrid approaches. This includes using the physics-based model output as additional data-driven input, learning the residual between physics-based model and real data, learning a surrogate of the physics-based model, or fine-tuning a surrogate model with real data. However, a comprehensive comparison of the inherent advantages of these hybrid approaches is still missing. The primary objective of this work is to evaluate four predominant hybrid approaches in building energy modeling through a real-world case study, with focus on indoor thermodynamics. To achieve this, we devise three scenarios reflecting common levels of building documentation and sensor availability, assess their performance, and analyze their explainability using hierarchical Shapley values. The real-world study reveals three notable findings. First, greater building documentation and sensor availability lead to higher prediction accuracy for hybrid approaches. Second, the performance of hybrid approaches depends on the type of building room, but the residual approach using a Feedforward Neural Network as data-driven sub-model performs best on average across all rooms. This hybrid approach also demonstrates a superior ability to leverage the simulation from the physics-based sub-model. Third, hierarchical Shapley values prove to be an effective tool for explaining and improving hybrid models while accounting for input correlations.

1. Introduction

In the last decade, the operation of buildings accounted for approximately 30% of global energy consumption and 26% of CO₂ emissions [1]. Over half of this consumption stems from the operation of building energy systems such as Heating, Ventilation and Air Conditioning (HVAC), as well as the electrical systems. This situation underscores the urgent need for measures to reduce energy consumption in the operation these systems. Fortunately, advancements in digitalization and sensor deployment provide a foundation for using analytical and machine learning tools to optimize the performance of building energy systems. On this basis, Building Energy Models (BEM) can be developed to simulate a building's real-world condition and predict future behaviour thereby enabling the recommendation of optimal control actions. However, a major challenge remains: the availability of building information and sensor data, particularly in terms of comprehensive building documentation, sensor coverage, and the length of recorded data. This lack of building information and sensor data complicates the reliable and accurate construction of BEMs but also hinders the widespread adoption of energy optimization strategies in buildings.

The Building Energy Model is a digital representation of a building designed for simulating energy and thermodynamics. It is constructed based on various characteristics of the building, including building geometry, material properties, installed energy systems, and operational inputs such as weather conditions, HVAC operation, and occupancy schedules [2]. To accurately reflect real-world conditions, the BEM is initially calibrated with sensor data to ensure faithful representation of the building and its energy systems. Once calibrated, the BEM can predict building operational performance and indoor temperature evolution across different time scales such as quarter-hourly or hourly resolution. Its comprehensive predictive capabilities make the BEM a versatile tool for various applications in building planning

*Corresponding author

 leandro.vonkrannichfeldt@epfl.ch (L.V. Krannichfeldt); olga.fink@epfl.ch (O. Fink)
ORCID(s): 0000-0001-8563-8086 (L.V. Krannichfeldt)

and operations. In retrofitting studies, it serves as an evaluation tool to assess potential measures for improving energy efficiency [3]. In building operations, it provides detailed temperature predictions as basis for control algorithms, enabling the optimization of energy system operations [4].

Classical BEMs are physics-based models that use a system of differential equations to represent all building subsystems and their interactions. This includes equations for indoor heat balance, HVAC dynamics, and incident solar radiation. These models, often referred to as physics-based models, provide insights into the underlying physical phenomena governing building performance [2]. However, the accuracy of these simulations can be compromised by the unavailability of detailed building information. Additionally, setting up a BEM can be a time-consuming process that requires significant expertise. A widely used physics-based modeling software in both academia and industry is EnergyPlus [5], which enables dynamic thermal simulations and supports the energy-efficient design and operation of buildings. In case of simplified building descriptions or the requirement to lower computational complexity, reduced-order physics-based models may be employed. These models consist of simplified physical descriptions in the form of differential equations paired with data-driven identification of model coefficients, such as thermal Resistance-Capacitance (RC) models [2].

More recent approaches of building energy modeling focus on data-driven methods, which utilize statistical and machine learning techniques such as Autoregressive Integrated Moving Average (ARIMA), Feedforward Neural Network (FFNN), Long Short-Term Memory (LSTM) and Convolutional Neural Network (CNN) [2]. These methods rely on sensor measurements to establish relationships between defined input and output variables. Commonly modelled relationships include those between building operation data – such as energy consumption or temperature – and the corresponding sensor readings. Since these models are applied to directly data, their underlying mechanisms are not easily accessible, classifying them as data-driven models. Furthermore, their complexity reduces interpretability. In such cases, post-hoc explainability methods like Shapley values [6], can be used to analyze model predictions. Unlike physics-based models, data-driven approaches do not require detailed physical building information or the calibration of physical parameters, making them easier to set up as digital twins. However, their performance is highly dependent on the quantity and quality of the available measurement data. Despite this dependency, data-driven models have demonstrated high accuracy in numerous studies and are particularly well-suited for modeling buildings at an urban scale, thanks to their reduced configuration time [7].

An emerging category of approaches for building energy modeling is known as hybrid or physics-induced modeling, which combines elements from physics-based and data-driven methods. These approaches offer significant advantages, particularly in scenarios where sensor data or detailed documentation is lacking.

Several research studies aim to combine reduced-order physics-based models with data-driven models through two general strategies. The first strategy involves formulating a loss function based on the reduced-order model to train the data-driven model. A prominent example is the use of Physics-informed Neural Network (PINN), where a physics-informed loss function is devised based on RC model thermodynamics in order to train a FFNN [8, 9, 10]. The second strategy consists of incorporating reduced-order model elements into a data-driven model architecture. A number of works model building dynamics with a State-Space model framework and parameterize state and/or observation equation with FFNN [11], Neural Ordinary Differential Equations [12] or Graph Neural Networks [13]. However, ensuring physical consistency still remains a challenge in aforementioned strategies [14].

Another line of work researches the combination of high-fidelity physics-based models with data-driven models. We identify four distinct approaches in the context of our research: assistant, residual, surrogate, and augmentation. In the **assistant strategy**, the output from a physics-based model is used as an additional input to the data-driven model [15, 16] or conversely, the data-driven model can provide inputs or corrections to the physics-based model [17, 18, 19]. This additional input may provide valuable context information, but also increases the number of input features. The **residual strategy** involves using a data-driven model to learn the residuals between the output of a physics-based model and actual observed data [20, 21, 22, 23]. This approach aims to capture unmodelled physical phenomena and variations in the data that the physics-based model may not fully account for. It is particularly useful when certain inputs are not reliably represented in the data or when incorporating domain knowledge with a physical reference input is necessary. In the **surrogate strategy**, a data-driven model is trained to replace the physics-based model by using the same inputs, with the physics-based model's simulations serving as the target outputs [24, 25, 26, 27, 28]. The primary motivation for this approach is to reduce computation time, allowing the data-driven model to perform simulations that would otherwise be time-consuming with the physics-based model. Nevertheless, it relies on a sufficiently accurate simulator. The **augmentation strategy** augments the real data with simulated data from a physics-based model, training the data-driven model on this augmented dataset and subsequently adapting it to real-world situations [29, 30, 31, 32].

This augmentation strategy is particularly advantageous when little to no real-world data is available, as it allows the model to leverage simulated data to improve its accuracy and generalization capabilities. However, this approach may suffer from performance degradation if there is a significant disparity between simulated and real data. An overview of the different characteristics of hybrid approaches in the context of our research is shown in Figure 1.

Several studies investigate the dependency of hybrid models on documentation and sensor measurements. For example, various levels of building documentation are explored in [15] using an assistant methodology that combines IDA-ICE software and Gradient Boosting Regression Trees (GBRT). In scenarios with limited sensor data, [33] employs a Surrogate-FFNN model based on EnergyPlus simulations to assess performance with varying data availability – 100%, 30% and 20%, or even less [34]. Additionally, [35] explores the impact of seasonally limited data using an Augmentation-FFNN-CNN model implemented through the MATLAB toolbox CARNOT [36]. Few research studies address the explainability of hybrid models. For example, [37] evaluates a Surrogate-Random Forest model trained on simulated data from EnergyPlus using Pearson correlation and Gini importance scores to assess feature relevance. Similarly, [38] enhances the interpretability of a Surrogate-GBRT model trained on simulated data from EnergyPlus by incorporating a causal inference framework, thereby making the hybrid model inherently more transparent.

Although hybrid approaches in BEM are gaining increasing attention, three significant research gaps remain. First, most recent studies focus on developing new hybrid methods within specific data contexts, yet there is a lack of a comprehensive research comparing the advantages and disadvantages of different hybrid approaches. A systematic evaluation of these methods is still missing, which limits our understanding of their relative strengths and weaknesses. Second, there are only few works that compare scenarios with limited building documentation or sensor data. Third, the majority of existing literature primarily evaluates hybrid models in terms of accuracy, with less attention given to the explainability of these approaches. Greater emphasis on explainability is crucial for understanding the hybrid models general behaviour, uncovering model biases of the physics-based sub-model and building trust for real-world application. Moreover, due to environmental and operational physical dependencies, sensor measurements exhibits interaction effects that are reflected in the model features. As a consequence, the joint influence of feature groups and non-linear interactions between features impact model predictions.

These research gaps highlight the need for more comparative studies and a deeper exploration of how hybrid BEMs perform under varying levels of data availability and quantity. We address these research gaps by conducting a comprehensive study of hybrid approaches in a real-world setting. For explainability, we opt for post-hoc explanation of model predictions, given the complexity of the investigated models. We introduce the hierarchical Shapley value as a suitable framework for our setting, as it effectively assigns feature contributions to correlated feature groups within the original output unit. In our study, we focus on the thermal modeling aspect of the BEM to predict indoor thermodynamics for two reasons. Firstly, the understanding of thermodynamics forms the foundation for all energy related calculations, also in physics-based models. Secondly, the focus on thermodynamics allows for a clear effect modeling and facilitated model analysis. Furthermore, we concentrate on a high-fidelity physics-based model for the construction of hybrid models. This paper tries to address the previously mentioned research gaps by making the following three main contributions:

- We enhance the understanding of hybrid building energy models by investigating and comparing four predominant hybrid approaches across three challenging real-world scenarios, each characterized by varying levels of building documentation and sensor data availability.
- We apply a hierarchical Shapley value framework to an agglomerative clustering analysis using Pearson's distance metric, providing valuable insights into the nature of hybrid models while accounting for the correlations. This also allows to investigate potential model biases of the physics-based part such as a bias at higher outdoor temperatures.
- We examine and compare performance of the four hybrid approaches in a limited training data setting, offering a detailed analysis of their dependency on data quantity and their robustness under constrained conditions.

The remainder of this paper is organized as follows: Section 2 outlines the methodology used in this study. Section 3 introduces the data set-up and implementation details of the hybrid approaches. Section 4 conducts case studies across various documentation and sensor scenarios and analyzes the results. Finally, Section 5 draws conclusions and provides an outlook on future research directions.

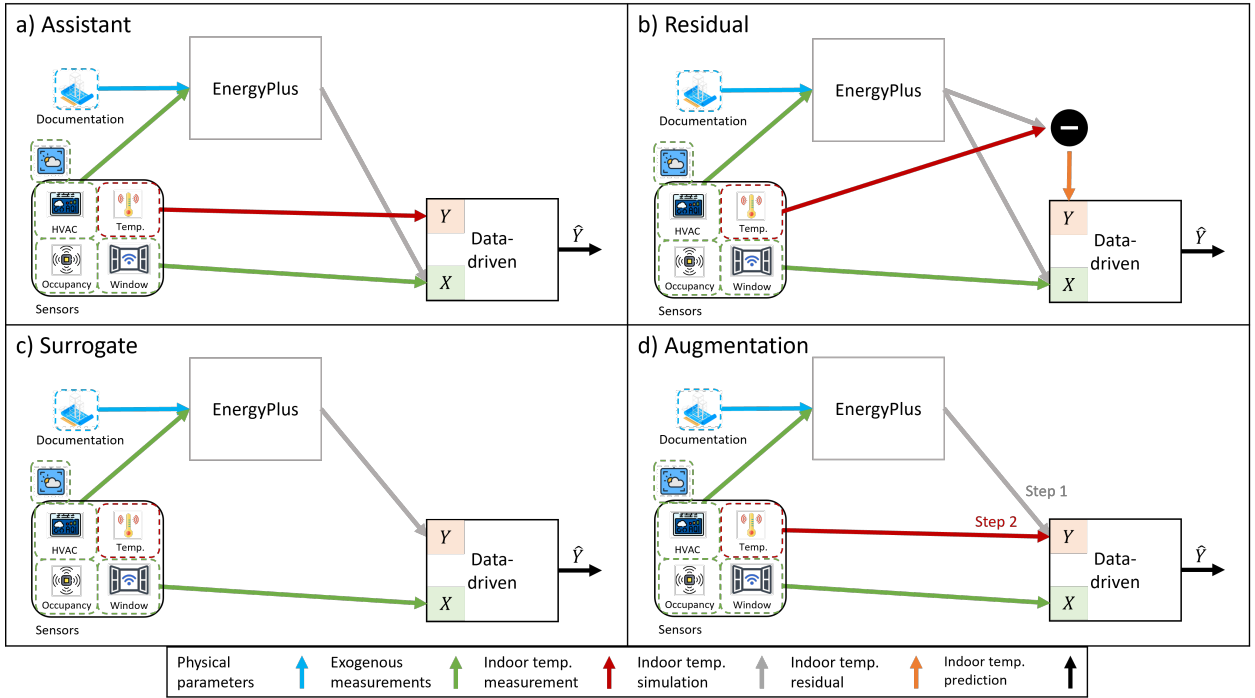


Figure 1: Overview of the different hybrid approaches with physics-based EnergyPlus and data-driven combination. The data sources are indicated as building documentation and sensors with various sensor groups. The corresponding data flows are indicated by colored arrows, which meanings are given in the legend at the figure bottom. The green exogenous data arrow indicates all the sensor measurements apart from the indoor room temperature. X and Y denote the input features and target variables of the data-driven model for learning purposes. \hat{Y} represents the hybrid model's indoor temperature prediction. Note that the augmentation approach involves a two-step learning procedure. While step 1 indicates the learning on simulated data, step 2 denotes the fine-tuning on real indoor temperature.

2. Methodology

Our methodology consists of combining a physics-based EnergyPlus model with a data-driven model in four prevalent combinations. We then proceed to evaluate these combinations based on accuracy using standard accuracy metrics, explainability using hierarchical Shapley values, and data dependency under different documentation and sensor availability scenarios.

2.1. Hybrid model

In our research, we evaluate the four most prevalent forms of combining physics-based and data-driven models in building energy modeling, shown in Figure 1. The **assistant approach** incorporates the indoor temperature predictions from the physics-based model as an additional input to the data-driven model. The **residual approach** involves using a data-driven model to learn the indoor temperature residuals – the differences between the physics-based model's predictions and the real indoor temperatures. The **surrogate approach** aims to train a data-driven model to fully replace the physics-based model for indoor temperature prediction, taking the physics-based simulation as training label. Finally, the **augmentation approach** takes this step further by fine-tuning the data-driven model with real data following its initial pre-training as a surrogate.

The corresponding algebraic equations for these hybrid models are given as:

$$\mathbf{f}_{assistant}(\mathbf{x}) = \mathbf{f}_{dd}(\mathbf{x}, \mathbf{f}_{EP}(\mathbf{x})), \quad l_{dd}(\mathbf{y}, \mathbf{f}_{assistant}(\mathbf{x})) \quad (1)$$

$$\mathbf{f}_{residual}(\mathbf{x}) = \mathbf{f}_{dd}(\mathbf{x}, \mathbf{f}_{EP}(\mathbf{x})), \quad l_{dd}(\mathbf{y} - \mathbf{f}_{EP}(\mathbf{x}), \mathbf{f}_{residual}(\mathbf{x})) \quad (2)$$

$$\mathbf{f}_{surrogate}(\mathbf{x}) = \mathbf{f}_{dd}(\mathbf{x}, \mathbf{f}_{EP}(\mathbf{x})), \quad l_{dd}(\mathbf{f}_{EP}(\mathbf{x}), \mathbf{f}_{surrogate}(\mathbf{x})) \quad (3)$$

$$\mathbf{f}_{augmentation}(\mathbf{x}) = \mathbf{f}_{surrogate}(\mathbf{x}, \mathbf{f}_{EP}(\mathbf{x})), \quad l_{dd}(\mathbf{y}, \mathbf{f}_{augmentation}(\mathbf{x})) \quad (4)$$

where \mathbf{f}_{EP} and \mathbf{f}_{dd} are the physics-based EnergyPlus and data-driven prediction functions, \mathbf{x} is a sample with the corresponding feature dimension, \mathbf{y} is the target with real indoor temperatures, and l_{dd} is the data-driven loss function. We employ all four approaches in our case study and compare them extensively.

2.2. Physics-based models

As our physics-based model, we utilize the widely recognized open-access building simulation software EnergyPlus (EP) [5] to construct a comprehensive building energy model, as depicted in Figure 2. EnergyPlus simulates the building and its subsystems using a system of differential equations. These modules include equations for the building envelope, indoor heat balance, mass balance, HVAC fluid dynamics, lighting system, window performance, and weather conditions. To set-up the EP model, the building geometry and physical parameters are curated from the building documentation and provided in an Intermediate Data Format file. Alongside weather data formatted in the EnergyPlus weather file, these inputs allow the internal simulation manager to accurately simulate the building's dynamics behaviour. Once the multi-zone building model is set up, its parameters are calibrated by aligning the real target variable with the simulation output using the sensor data from the building and individual rooms. This procedure ensures accurate simulation of thermodynamics within the building. In case of less detailed building information, an archetypal EnergyPlus model can be constructed. For this purpose, we use the archetype framework Cesar-P [39, 40] for automated model construction. On the basis of building footprint, height, year of construction and building type, the Cesar-P framework constructs a suitable archetypal Energyplus model with pre-defined material and geometry settings.

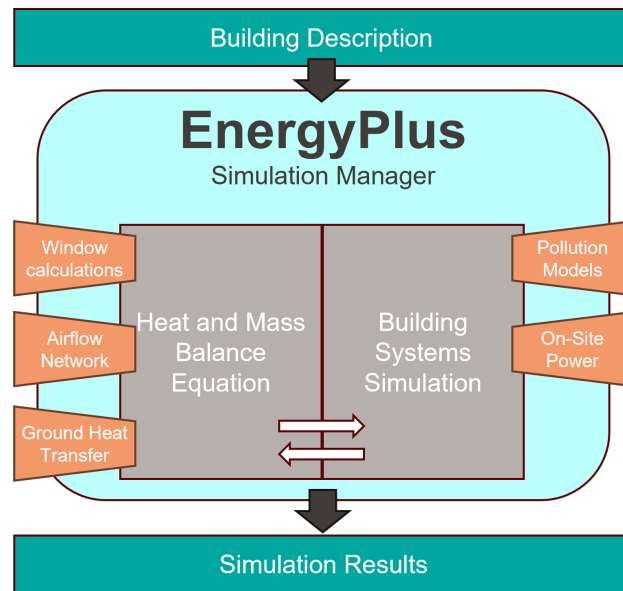


Figure 2: Overview of the EnergyPlus workflow with modules, adapted from [5].

2.3. Data-driven models

In the case of data-driven models we investigate Linear Regression (LR), Feedforward Neural Network (FFNN) and Random Forest (RF). We choose the LR due to its simplicity as well as strong baseline performance. The FFNN is chosen for its popularity and adequacy for regression problems. It also has computational advantages compared to kernel-based methods such as Support Vector Regression. The RF is selected as a representative of the tree ensemble models that are widely used in regression problems for their accuracy. Moreover, both FFNN and RF are able to represent the building thermodynamics of all rooms within a single model. A Recurrent Network architecture is not considered since no time-lagged features are used as input. This enables a direct comparison to the pure physics-based EnergyPlus simulation, which doesn't allow explicit time lag integration.

The multiple **Linear Regression** is defined by the Least Squares optimization problem [41]:

$$\min_{\mathbf{W}} \|\mathbf{W}\mathbf{X} - \mathbf{Y}\|^2 \quad (5)$$

The solution to this problem is given by:

$$\mathbf{W} = (\mathbf{X}^T \mathbf{X})^{-1} \mathbf{X} \mathbf{Y} \quad (6)$$

where $\mathbf{X} \in \mathbb{R}^{N \times d}$ is the feature matrix consisting of N samples and d features, $\mathbf{Y} \in \mathbb{R}^{N \times K}$ is the target matrix composed by N samples and K target variables, and $\mathbf{W} \in \mathbb{R}^{d \times K}$ are the regression coefficients. It is important to note that the solution to the Multiple Linear Regression decouples between the target variables into individual Linear Regression solutions per target. Thus, the prediction function for a target room temperature $\mathbf{y}^{(k)}$ given a sample \mathbf{x} is:

$$\mathbf{f}(\mathbf{x}) = \mathbf{W}_k \mathbf{x} \quad (7)$$

Regarding the **Feedforward Neural Network**, the model equations are defined by:

$$\mathbf{f}(\mathbf{x}) = \mathbf{z}^{(L)} \circ \mathbf{z}^{(L-1)} \circ \dots \circ \mathbf{z}^{(1)}(\mathbf{x}) \quad (8)$$

$$\mathbf{z}^{(k)} = \alpha^{(k)}(\mathbf{W}^{(k)} \mathbf{z}^{(k-1)} + \mathbf{b}^{(k)}) \quad (9)$$

$$\mathbf{z}^{(1)} = \alpha^{(1)}(\mathbf{W}^{(1)} \mathbf{x} + \mathbf{b}^{(1)}) \quad (10)$$

where, $\alpha^{(i)}$, $\mathbf{W}^{(i)}$, and $\mathbf{b}^{(i)}$ represent the activation function, network weights, and bias of the i -th layer, respectively. Further, the \circ -symbol denotes the composition of functions. The network weights are learned by using an optimizer to iteratively solve the optimization problem with stochastic approximation [41]:

$$\mathbf{W} = \arg \min_{\mathbf{W}} \frac{1}{N} \sum_{i=1}^N \|\mathbf{y}_i - \mathbf{f}(\mathbf{x}_i, \mathbf{W})\|^2 \quad (11)$$

The **Random Forest** regression works by averaging many unbiased tree models to reduce the overall model variance [41]. By denoting a regression tree as T_b , the model equation for B number of trees is given as:

$$\mathbf{f}(\mathbf{x}) = \frac{1}{B} \sum_{b=1}^B T_b(\mathbf{x}), \quad T_b(\mathbf{x}) = \sum_{j=1}^J \mathbf{c}_j \mathbb{1}_{\{\mathbf{x} \in R_j\}} \quad (12)$$

where R_j is a region in the feature space partition, \mathbf{c}_j are the constant values for the region R_j and $\mathbb{1}_{\{\cdot\}}$ represents the indicator function. The parameters are found by minimizing the following combinatorial optimization problem:

$$\mathbf{R}, \mathbf{c} = \arg \min_{\mathbf{R}, \mathbf{c}} \sum_{j=1}^J \sum_{\mathbf{x}_i \in R_j} \|\mathbf{y}_i - \mathbf{c}_j\|^2 \quad (13)$$

2.4. Explainability

We refer to explainability as the ability to describe and justify a model's predictions, especially for complex data-driven models, such as Deep Learning models used in this research [42]. In a combination of physics-based and data-driven models, the explainability of the data-driven model as well as of the interdependencies between the two sub-models is crucial for the overall understanding. In particular, we want to examine these two aspects through the lens of feature contributions for model predictions on a global level. In this way, we can assign feature importance to get a better understanding of the model's general behaviour, uncover model biases and potentially give suggestions whether to record particular sensor variables. To comprehensively explain the hybrid models, we employ a Shapley value framework [43] with the Shapley additive explanations (SHAP) package [6]. Given the challenge of correlated input features, we opt for a hierarchical Shapley value calculation [44]. In this approach, hierarchical Shapley values are recursively computed based on a predefined hierarchy. We establish this hierarchy using agglomerative clustering

[45], with Pearson's distance [46] as the distance metric. Consequently, the distance matrix \mathbf{D} can be expressed as follows:

$$\mathbf{D} = \mathbf{1} - \mathbf{R}_{\mathbf{XX}}, \quad \mathbf{R}_{\mathbf{XX}}^{(i,j)} = |\text{cov}(\mathbf{X}_i, \mathbf{X}_j) / (\sigma_i \sigma_j)| \quad (14)$$

where each entry of the absolute correlation matrix $\mathbf{R}_{\mathbf{XX}}$ represents the absolute value of the Pearson correlation between two feature columns. Here, cov denotes covariance and σ represents standard deviation. Subsequently, the hierarchical Shapley value ϕ_i of a specific feature i is computed as follows:

$$\phi_i(v, B) = \sum_{R \subseteq M \setminus \{k\}} \sum_{T \subseteq B_k \setminus \{i\}} \frac{1}{|M| |B_k|} \frac{1}{\binom{|M|-1}{|R|}} \frac{1}{\binom{|B_k|-1}{|T|}} [v(Q \cup T \cup \{i\}) - v(Q \cup T)] \quad (15)$$

where the norm $|\cdot|$ in this context denotes the size of a set, M is the set of clusters, $B = \{B_1, \dots, B_m\}$ represents the partition of features into clusters, B_k is the cluster containing feature i and k is the index of cluster containing feature i . R is a subset of clusters and the first binomial coefficient calculates the corresponding number of ways that to choose $|R|$ subsets out of $|M| - 1$ clusters. T is a subset of features and the second binomial coefficient calculates the corresponding number of ways that to choose $|T|$ features within cluster B_k from $|B_k| - 1$ features. $Q = \bigcup_{r \in R} B_r$ is a union of features in the clusters defined by R , and $v(\cdot) = \mathbb{E}[\mathbf{f}(\mathbf{X}) | \mathbf{X}_{(\cdot)}]$ is the expected prediction of a subset. Therefore, the term $v(Q \cup T \cup \{i\}) - v(Q \cup T)$ describes the marginal contribution of feature i when added to the union $Q \cup T$. In addition to the hierarchical Shapley values, we analyze the intrinsic interpretability of different models: Linear Regression through regression coefficients, Random Forest through Gini importance, and Neural Network through Jacobian matrix sensitivity. However, these intrinsic measures become less interpretable in the presence of feature interactions from correlated input features.

2.5. Evaluation metrics

For evaluating the accuracy of temperature predictions, we utilize the widely used metrics: Mean Absolute Error (MAE) for its insensitivity to outliers, Mean Absolute Percentage Error (MAPE) for its comparability across rooms as well as Root Mean Squared Error (RMSE) for its outlier penalization. These metrics are defined as follows:

$$\text{MAE} = \frac{1}{T} \sum_{t=1}^T |y_t - \hat{y}_t| \quad (16)$$

$$\text{MAPE} = \frac{1}{T} \sum_{t=1}^T \left| \frac{y_t - \hat{y}_t}{y_t} \right| \quad (17)$$

$$\text{RMSE} = \sqrt{\frac{1}{T} \sum_{t=1}^T (y_t - \hat{y}_t)^2} \quad (18)$$

where y_t and \hat{y}_t represent the real and predicted room temperatures at time t , across T time steps.

3. Case study

3.1. Dataset

The main subject of investigation is the inhabited experimental unit Urban Mining and Recycling (UMAR), located at the Swiss Federal Laboratories for Materials Science and Technology (Empa) in Dübendorf [47], as shown in Figure 3. In terms of representativeness, previous research indicates that the UMAR unit is representative of the average Swiss residential building stock around 2050 [48]. The unit comprises several rooms equipped with various indoor and outdoor sensors, which have been recording data over several years. Our study concentrates on the five most frequently

used rooms: two bedrooms (R272, R274), a living room (R273), and two bathrooms (R275, R276). The utility room is not regarded for our study. A comprehensive overview of all weather, building, and room sensors utilized in this study is provided in Table 2. The dataset for our case study is recorded at a 1-minute resolution for all sensor variables spanning the two years 2020 and 2021. For the whole dataset, the percentage of missing values is below 1%. After linearly interpolating the missing values, the dataset is aggregated to 15-minutes resolution. The dataset is split into a 50%/50% training/test set, with the year 2020 used for training and the year 2021 used for testing.



Figure 3: UMAR unit at Empa with two bedrooms, one living room and two bathrooms.

3.2. Documentation/sensor scenarios

The case study aims to investigate the performance of hybrid models in common real-world scenarios. To achieve this, we define commonly encountered levels of documentation (floor plan, construction information, ...) and sensor availability, as outlined in Table 1. The documentation level is categorized as either archetypal, using general information such as building layout, type, glazing ratio, and year of construction, or detailed, relying on comprehensive building documentation. Sensor availability is classified into three levels: weather, building and room, also detailed in Table 2. The weather-level includes only weather-related variables such as outdoor temperature and solar radiation. The building-level adds measurements for entire building, including total heating and cooling power. The room-level further includes room-specific variables such as temperature setpoints, occupancy, and shading. Each specific combination of documentation and sensor levels is referred to as a scenario. In our study, we focus on three typical scenarios: W-, WB- and WBR-scenario. In the W-scenario, we assume that only weather-related sensors are available as well as only basic building information. On this basis, we utilize the archetype framework Cesar-P [40] construct a simplified EnergyPlus model as physics-based model. In the WB-scenario, we consider having weather and general building related sensors as well as detailed construction information. In this case, we use an uncalibrated detailed EnergyPlus model, since a precise calibration without room sensors is not possible. In the WBR-scenario, we presume having access to weather, building and room sensors as well as detailed construction information. Here, we take a calibrated detailed EnergyPlus model to serve as the physics-based component in the hybrid models.

3.3. Model architecture

In our time series regression framework, we use all exogenous variables to predict the indoor temperatures of all rooms at the same time step. No time-lagged data is used as input to enable a direct comparison to the pure physics-based EnergyPlus simulation. Regarding the physics-based model, we use a Cesar-P model for the W-scenario and a detailed EnergyPlus model for the WB- and WBR-scenarios. The Cesar-P model is configured using parameters such as building footprint, type, age, heating system type, and glazing ratio and set up as a simplified EnergyPlus model. For the detailed EnergyPlus model, we employ the same model as described in [4], using an uncalibrated version for the WB-scenario and a fully calibrated version according to the authors's calibration cycle for the WBR-scenario. In both instances, each room is treated as a single temperature zone.

For the data-driven part, we compare three models of differing complexity: LR, FFNN and RF. While LR and RF

Documentation	Sensors		
	Weather	Weather/Building	Weather/Building/Room
Archetypal	W-scenario Cesar-P	-	-
Detailed	-	WB-scenario Uncalibrated EP	WBR-scenario Calibrated EP

Table 1: Documentation and sensor data settings with corresponding physics-based model part and scenario name.

Feature group	Feature variables
Datetime	Season, week (weekday/weekend), daytime (morning/afternoon/evening/night)
Weather	Drybulb & dewpoint temperature, diffuse & diffuse solar radiation, rel. humidity, wind direction & speed
Building	Total cooling & heating mass flows, network temperature, air-conditioning mode (cool/heat)
Room	Mass flow, temperature setpoint, occupancy, window position (closed/open), blinds position (up/down)

Table 2: Feature groups with corresponding feature variables. Note that the datetime group is used for all W-, WB- and WBR-scenario.

implementations are used from Scikit-learn [49], the FFNN is implemented in Pytorch [50]. All three models are trained on standardized feature inputs. The LR model used is a multiple ordinary least squares regression with an intercept. The FFNN consists of two layers with 128 neurons activated by the sigmoid function. It is trained using a batch size of 32, with a maximum of 1000 epochs, early stopping with a patience of 10, and a validation split of 20%. The model is optimized using the Adam optimizer and the mean squared error loss function. In case of the RF, the number of forest trees is 300, the splitting criterion squared error, the minimum samples split 2 and minimum samples leaf 1. The specific FFNN and RF architectures are determined through hyperparameter grid search for the data-driven case. The chosen hyperparameters are maintained consistent across all hybrid approaches as well as all documentation/sensor scenario in order to isolate the effects of each experimental condition.

In integrating the physics-based and data-driven components, we explore four approaches: residual, assistant, surrogate and augmentation. For the augmentation approach, fine-tuning is performed with early stopping set to a patience of 3. Fine-tuning of the Augmentation-LR model is achieved by updating the LR weights using the Adam optimizer. The fine-tuning in case of the Augmentation-RF is achieved by using the previously fitted trees on the simulated data as warm start and adding 100 more trees for learning on the real data.

4. Results and analysis

4.1. Prediction performance

In order to comprehensively evaluate the hybrid models' prediction performance in real-world settings, we explore their performance in three different documentation/sensor scenarios. The results for the three documentation/sensor scenarios employing the time series regression framework are illustrated in Figure 4, presented as a MAPE boxplot across all rooms. Across all methods, the average MAPE (indicated by the green triangles) decreases as the level of documentation and sensor data increases from W-scenario to WBR-scenario. Notably, for the best performing method, Residual-FFNN, the MAPE improves by 0.88%, decreasing from 4.55 % in the W-scenario to 3.67 % in the WBR-scenario. This indicates that while the weather features and archetypal building characteristics provide a robust foundation for prediction, significant gains are achieved through the inclusion of more more sensors and documentation data. Furthermore, all hybrid methods, except for the surrogate models, outperform the EP simulator in terms of MAPE. Across all scenarios, the hybrid models exhibit performance comparable to the purely data-driven LR and FFNN. Nevertheless, we can see a slight performance advantage for the Residual-FFNN in the WBR-scenario.

Figure 5 presents the performance of the WBR scenario, broken down by room. While the Residual-FFNN demonstrates the best overall performance (indicated by the grey-dotted line), there are notable variations across different room types. Specifically, the Residual-FFNN achieves the lowest MAPE in bedroom 274, whereas the Residual-RF performs better in the living room 273 and bedroom 272. For the two bathrooms, the Augmentation-FFNN yields the lowest MAPE for bathroom 276 and the data-driven RF the best MAPE performance for bathroom

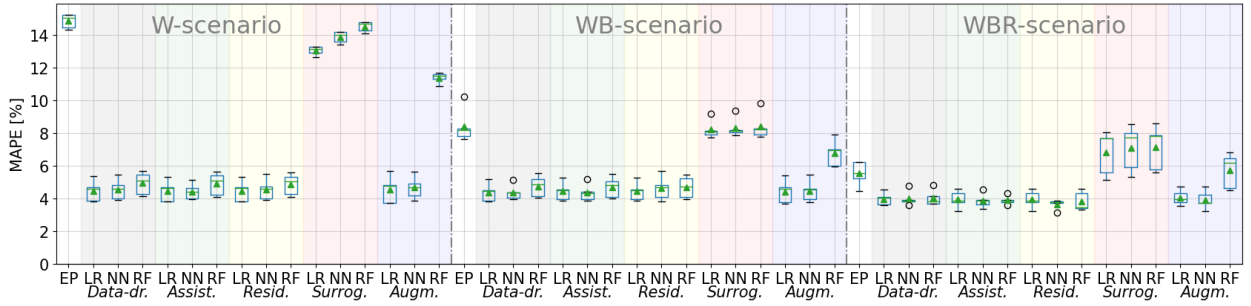


Figure 4: MAPE boxplot for the three scenarios W, WB and WBR between real indoor temperature and model prediction. The green triangle and line denote mean resp. median of the error distribution.

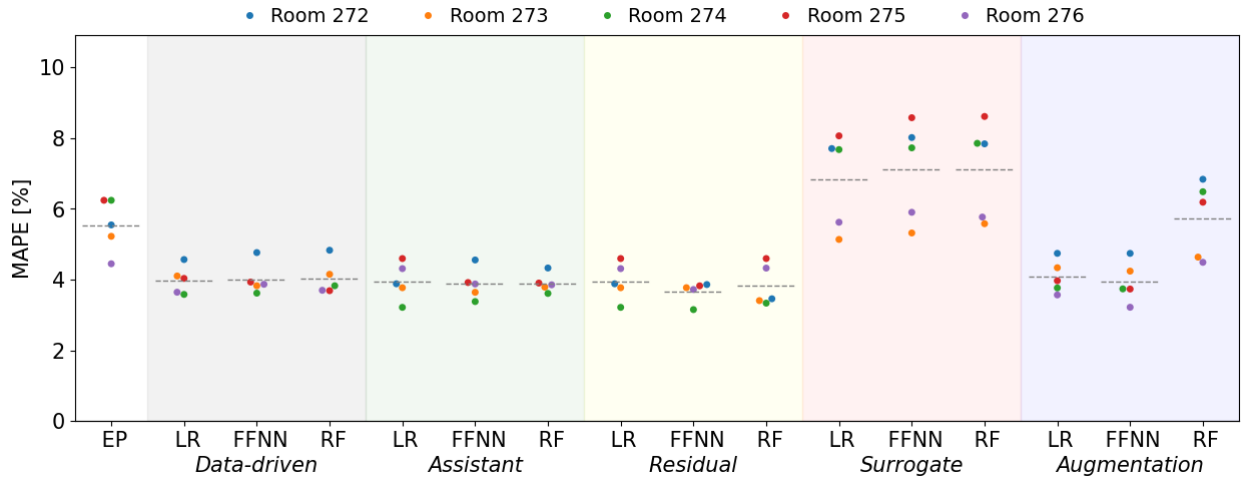


Figure 5: MAPE for all rooms, hybrid approaches as well as pure physics-based and data-driven models in the WBR-scenario. The grey-dotted line indicates the mean MAPE across all rooms.

275. An example of the Residual-FFNN’s superior performance is highlighted in Figure 6. During extended window openings from March 4th to 7th and March 11th to 15th (shaded in grey), the Residual-FFNN accurately captures the extreme temperature fluctuations by leveraging the EP model. In contrast, the purely data-driven model and other hybrid approaches fail to predict this behaviour effectively. The FFNN shows difficulties to learn relationships that generalize to such extreme window behaviour. The Assistant-FFNN approach seems unable to beneficially use the EP simulation as feature, even deteriorating performance compared to FFNN in these cases. In the augmentation approach, we observe a slight improvement over FFNN, indicating that the two-step learning approach can bring advantages in such situations. A similar effect can be observed in the residual approaches of LR and RF Figure 16 and Figure 17. The mean performance of all methods for MAPE, MAE and RMSE is given in Figure 5.

Figure 7 presents the average MAPE across rooms, grouped by month, for the hybrid models. Two notable observations can be made. Firstly, March and April exhibit a higher error rate, exceeding 4 % MAPE for all models. This is due to extended periods of open windows in the bedrooms and living room, which cause a drop in room temperature and trigger the heating system to compensate. These extreme fluctuations are challenging for all models to accurately capture. Secondly, in November and December, the EP model performs competitively with the other models compared to the rest of the year. An explanation for this is the rental situation of UMAR, as the unit was uninhabited in winter 2021. Consequently, the temperature patterns in November and December 2021 were more regular, making it easier for the EP model to simulate. In contrast, the other models were trained on data from 2020 when the unit was inhabited during winter. This makes it harder for them to generalize to an uninhabited period.

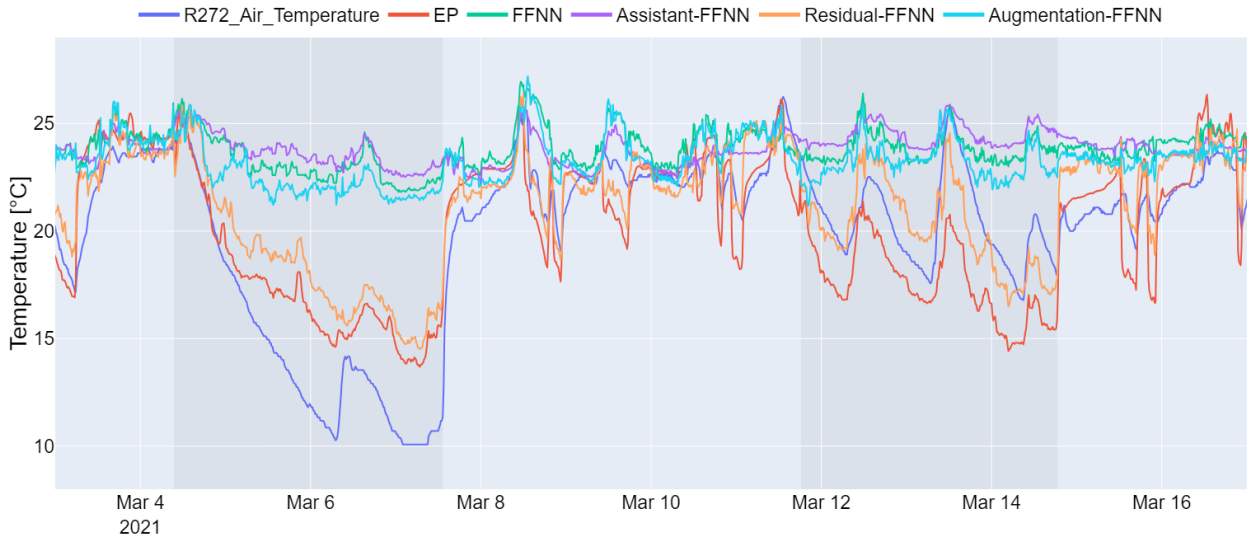


Figure 6: Forecast visualization for a selection of hybrid models for bedroom 272 in the WBR-scenario. The predictions of the surrogate approach are omitted for better visibility. The grey shaded areas indicate the extended period of window openings.

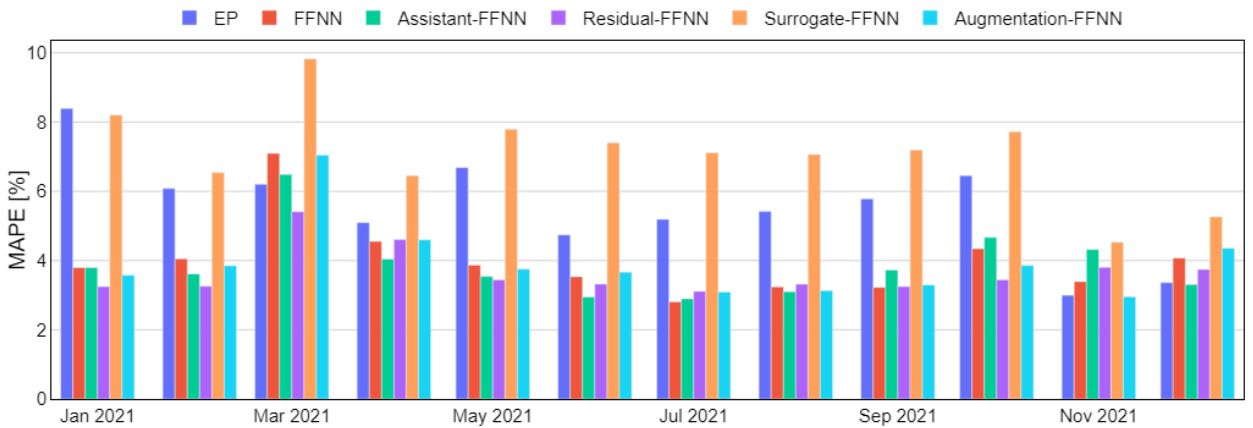


Figure 7: Average MAPE across rooms and grouped by month for the hybrid FFNN models.

4.2. Influence of historical sensor data

The influence of historical sensor data can give insights into the impact of short- and long-term effects on prediction performance. To this end, we examine a Long Short-term Memory (LSTM) Network [51]. To be comparable to the FFNN, we employ a two layer network with 128 neurons each and train it in the same fashion.

In Figure 8, we display the MAPE for the hybrid approaches with FFNN and LSTM. We observe that the Residual approach shows the best overall performance, with a slight advantage of Residual-FFNN over Residual-LSTM. This could indicate that the residual approach has a superior ability to leverage short-term historical effects. Nevertheless, when looking at the room-wise performance, we see that the pure data-driven models outperform the residual approach for the two bathrooms. This phenomenon could be traced back again to the peculiar dynamics of the bathrooms, complicating their physics-based modeling.

Figure 9 shows the MAPE performance of the Residual-FFNN and Residual-LSTM for increasing hours of history. In order to isolate the effect of history integration, the model architectures are kept constant. We observe that the lowest error is achieved by the Residual-FFNN with 1 hour of historical sensor data. Interestingly, the Residual-LSTM also

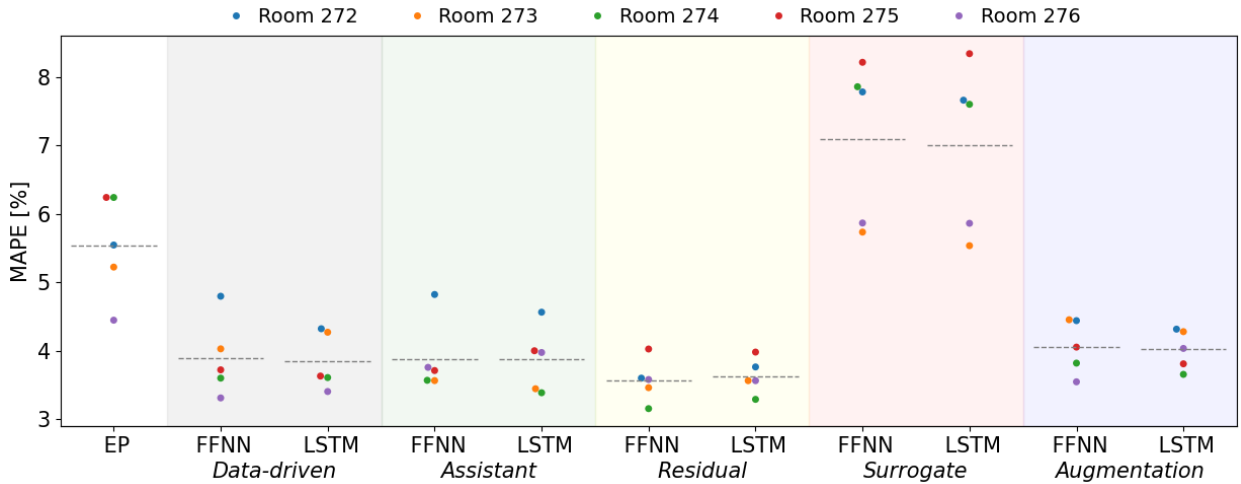


Figure 8: Comparison between hybrid approaches of FFNN and LSTM for the case of one hour history integration.

displays its best performance with 1 hour history integration. This could indicate that short-term effects in UMAR such as solar radiation are predominant, and integrating longer-term effects may not bring additional benefits. Further, we observe a large performance degradation with increasing hours for Residual-FFNN. This suggests an underfitting of the model, since one additional hour of history corresponds to an addition of about 200 features. Conversely, the Residual-LSTM has a superior ability to integrate the historical data having a substantially lower error for increasing hours.

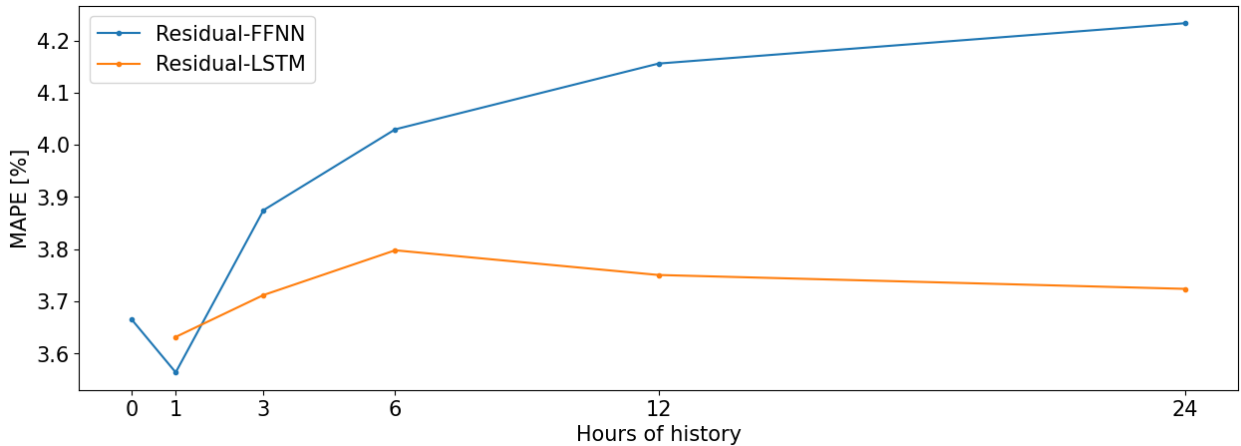


Figure 9: Comparison between Residual-FFNN and Residual-LSTM when including different hours of sensor history. Note that 0 hours of history represents the direct input-output mapping from features to target at the same time step.

4.3. Explainability within model

In order to improve the understanding of the data-driven model as well as of the interdependencies between the physics-based and data-driven model, we investigate the models by using hierarchical Shapley Value framework to explain their predictions. Our analysis focuses on the WBR-scenario due the highest documentation and sensor availability level. Moreover, we concentrate on living room 273 because it's the largest room and on the Residual-FFNN given its best average performance across all rooms. Figure 10 presents the SHAP beeswarm plot for the hierarchical Shapley values, highlighting the 10 most influential features for living room 273 as identified by the Residual-FFNN model. Among the top features are the simulated EP input, weather variables (solar radiation, relative

humidity, dew-point temperature), as well as room-specific variables like occupancy and shading. It is intuitive that the simulated EP inputs play a key role in a residual approach. Additionally, the significant contribution of room-level variables underscores their importance in model performance. The high importance of weather variables suggests that the residual approach compensates for weather variations not fully captured by the EP model.

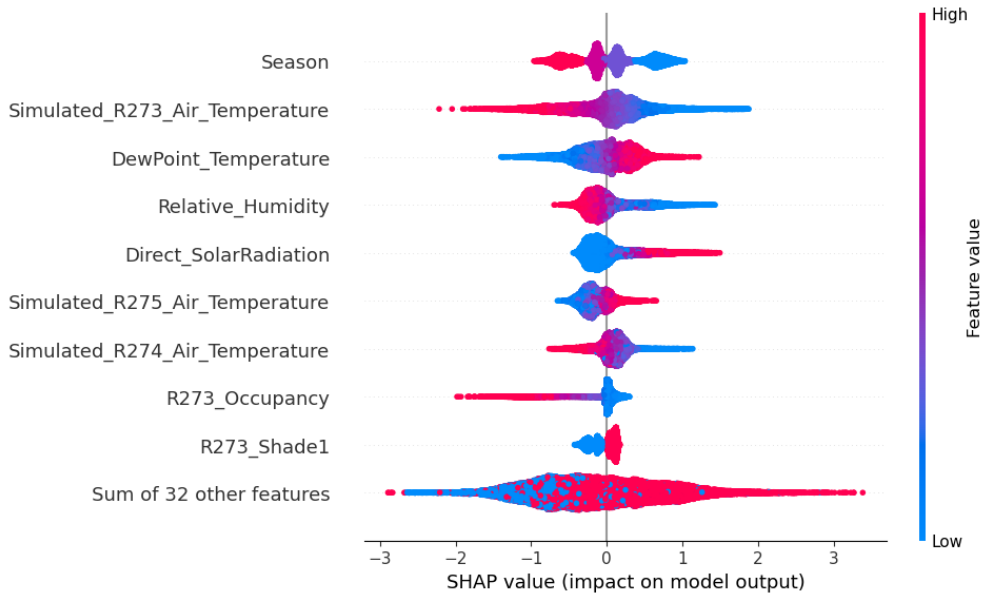


Figure 10: SHAP beeswarm plot with 10 most influential features for living room 273 for the Residual-FFNN in the WBR-scenario.

Figure 11 presents the SHAP dependence plot for living room 273, highlighting the second most important feature (Simulated air temperature) according to Figure 10. Note that the Shapley value represents the average contribution to the output and in this case the contribution in temperature degrees to the residual correction. The plot reveals that when the simulated temperature input exceeds a threshold of 24.6°C, the contribution to the residual correction is generally negative. Below this threshold, the contribution to the correction is positive. Examining the dry-bulb temperature coloring, we observe that contributions to residual corrections for higher temperatures tend to be negative and up to a correction contribution of -2 degrees, which may suggest a bias in the EP model at higher temperatures. This insight could serve as a basis for improving the EP model.

Figure 12 displays the hierarchical Shapley dendrogram for the inputs of the best-performing method, Residual-FFNN. With a few minor exceptions, four distinct groups can be identified. The orange cluster is composed mainly of outdoor temperature and room mass flow variables. The green cluster includes wind, window, and occupancy variables. The red and violet clusters are dominated by EP simulated inputs, solar radiation, and relative humidity, while the brown group consists of setpoints and shading variables. Notably, Table 3 exposes that the red cluster holds the highest relative importance among all clusters for room 273. This indicates that solar radiation, simulated air temperatures and relative humidity are the most impactful input group. The strong influence of solar radiation is consistent with the observation that the living room has three large windows. At the same time, the importance of the simulated air temperatures can be attributed to the nature of the residual model. If we cut the dendrogram at the second level, the red, violet and brown groups together have an aggregated hierarchical Shapley value that is more than double that of the combined orange and green clusters for room 273. We can interpret features directly related to indoor temperature (simulated air temperatures and temperature set points) as well as irradiation related features (solar radiation and shading) contribute significantly more on average than outside temperature, wind features, window openings and occupancy. A similar effect is observed for the two bedrooms, except that the violet group has gained importance due to the simulated temperature of the respective bedrooms being in this group. In case of the bathrooms, we notice a decrease of importance in all groups besides the red cluster, of which the simulated temperatures of bathrooms are part of. Such an effect can be attributed to the more isolated dynamics of the bathrooms having no windows.

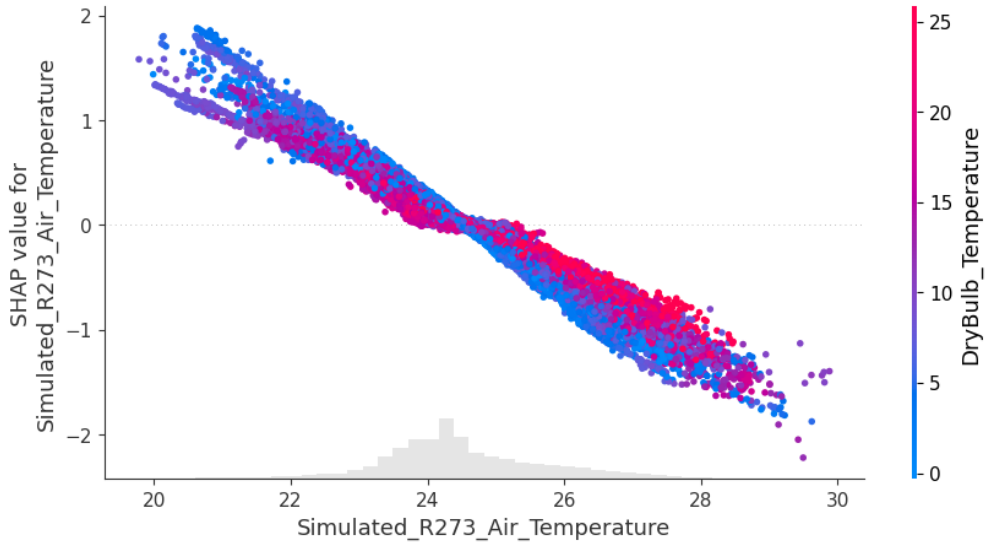


Figure 11: SHAP dependence plot for living room 273 according to Residual-FFNN showing the dependence between the simulated EP input and the corresponding Shapley value colored by dry-bulb temperature.

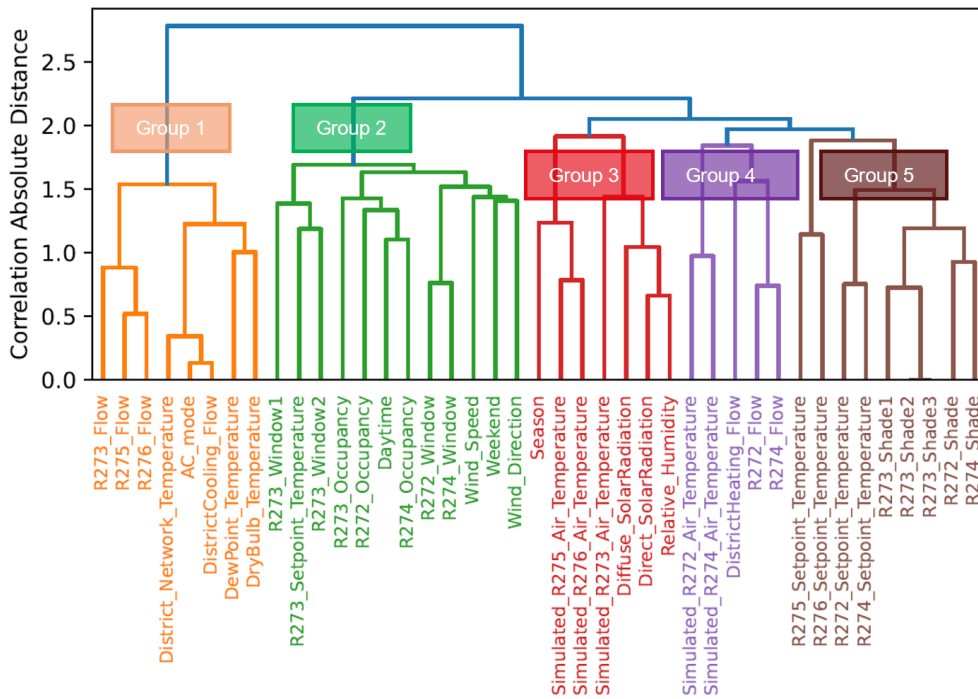


Figure 12: Dendrogram for input of Residual-FFNN in the WBR-scenario.

4.4. Explainability comparison between models

In order to compare the influences of the input cluster groups across the different hybrid approaches, Figure 13 shows the averaged absolute hierarchical Shapley values across rooms for LR, FFNN and RF. Note that the cluster groups of the assistant and residual approaches follow the same form shown in Figure 12 due to the additional simulated input, and are henceforth denoted as Assisted/Residual-clustering (AR-clustering). The data-driven, augmentation and surrogate approach follow the same form given in Figure 18 having no additional simulated input and are denoted

	Group 1	Group 2	Group 3	Group 4	Group 5
Bedroom 272	0.61	0.40	0.84	0.77	0.75
Living room 273	0.73	0.49	1.55	0.36	0.75
Bedroom 274	0.47	0.38	0.96	0.80	0.52
Bathroom 275	0.20	0.27	0.88	0.13	0.33
Bathroom 276	0.30	0.20	0.69	0.17	0.36
Room average	0.46	0.35	0.98	0.45	0.54

Table 3: Hierarchical Shapley values for all dendrogram groups in the case of the Residual-FFNN.

as Data-driven/Augmentation/Surrogate-clustering (DAS-clustering). In principle, the DAS-clustering resembles the AR-clustering for most parts, except for the absence of simulated inputs, the violet group being dissolved into the orange and green one as well as two set point input being merged into the green cluster. Moreover, note that the values between LR, FFNN, and RF hybrid approaches should not be compared directly but only in relative terms, since the Shapley value calculation is highly dependent on the model's inner workings. The most informative observation in Figure 13 is the high importance of the red cluster relative to the other clusters in case of the assistant and residual approaches for RL, FFNN and RF. In contrast, the DAS-clustering bar plots show a more balanced picture with the orange group having the highest importance. This suggests that the assistant and residual approach are provided with most parts of the dynamics through the simulated inputs in the red group, while the data-driven, augmentation and surrogate approach have to learn the thermodynamics primarily through the sensor data.

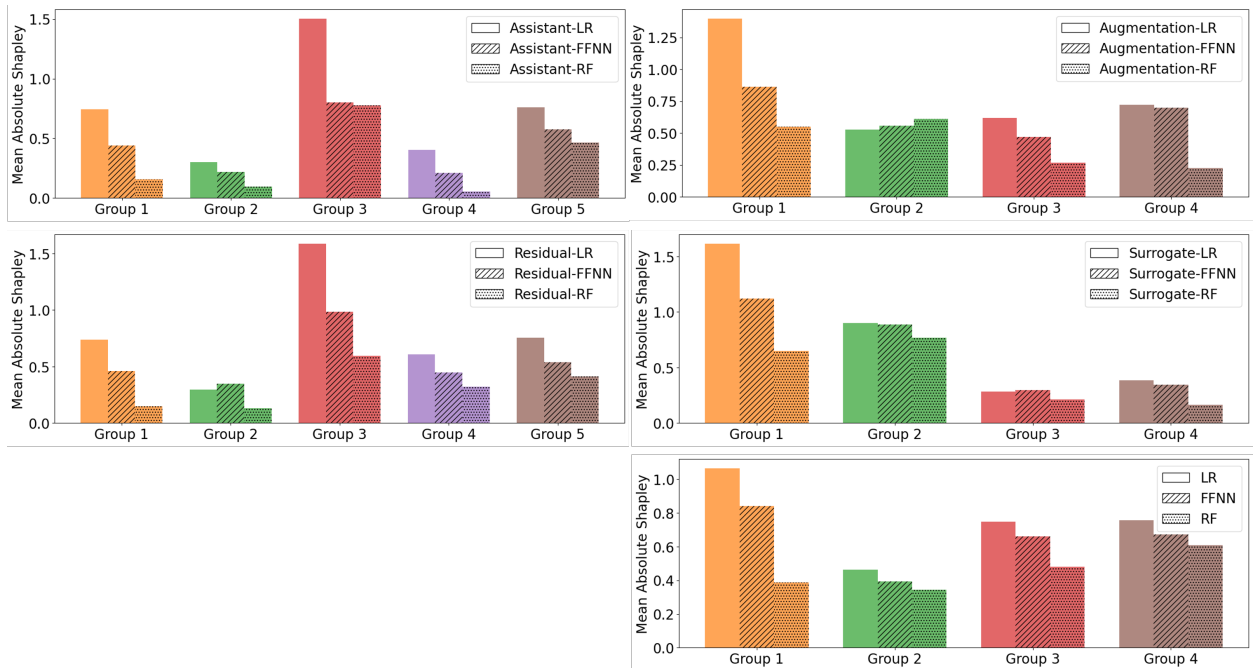


Figure 13: Averaged absolute hierarchical Shapley value across rooms for each cluster group and hybrid approach. Note that values between different models should only be compared relative to each other.

It is also instructive to compare the native importance measures of LR, FFNN and RF with the hierarchical Shapley values. In case of LR, the linear effects are computed as the regression coefficients multiplied by the features for each sample. Linear effects are very simple to calculate, but do not account for feature interactions. A way to quantify importance for the FFNN represents the Jacobian sensitivity, where the change of the output with respect to the input is calculated for each sample. The Jacobian reflects the direct influence of each input to output, but does not capture feature interactions and assumes a local linear approximation of the input-output relationship. For the RF, we can calculate the mean decrease in impurity calculated as the total reduction of the splitting criterion induced by a specific feature.

		Model Native	Hierarchical Shapley
Linear Effect - LR	Rank 1	Simulated_R275_Air_Temperature	Simulated_R275_Air_Temperature
	Rank 2	Simulated_R276_Air_Temperature	Simulated_R276_Air_Temperature
	Rank 3	Relative_Humidity	DewPoint_Temperature
	Rank 4	R274_Shade	Simulated_R274_Air_Temperature
	Rank 5	DewPoint_Temperature	Simulated_R272_Air_Temperature
Jacobian Sensitivity - FFNN	Rank 1	Simulated_R272_Air_Temperature	Simulated_R275_Air_Temperature
	Rank 2	Simulated_R276_Air_Temperature	Season
	Rank 3	Simulated_R273_Air_Temperature	Simulated_R272_Air_Temperature
	Rank 4	Simulated_R275_Air_Temperature	Simulated_R274_Air_Temperature
	Rank 5	Season	Simulated_R273_Air_Temperature
Gini Impurity - RF	Rank 1	Simulated_R276_Air_Temperature	Season
	Rank 2	Simulated_R272_Air_Temperature	Simulated_R276_Air_Temperature
	Rank 3	Season	Simulated_R272_Air_Temperature
	Rank 4	DistrictHeating_Flow	Simulated_R275_Air_Temperature
	Rank 5	Simulated_R275_Air_Temperature	DistrictHeating_Flow

Table 4: Model native importance measures contrasted with hierarchical Shapley values for Residual-LR, -FFNN and -RF

A drawback of the mean decrease impurity calculation is that features with many unique values can be overly favored since they have more opportunities to reduce the impurity. Moreover, the mean decrease impurity does not account for feature interactions. A ranking comparison of the five most important features for the model native importance measures and the hierarchical Shapley values in the case of the residual approach is given in Table 4. We see that in case of the linear effects of LR and Jacobian sensitivity of FFNN, three respectively four out of five features actually overlap in the top 5 ranking. In contrast, the mean impurity decrease of RF has a perfect overlap for the top 5 positions. We can conclude that even though the model native importance measures do not account for feature interactions, the top features are relatively well captured. Furthermore, the mean impurity decrease of RF seems to be the most reliable measure in this regard. The complete feature importance plots can be found in Figure 23, Figure 24 and Figure 25.

4.5. Impact of data quantity on performance

In practice, building sensor data may not be abundantly available due to recent sensor installation, temporary sensor deployment or sensor failures. In this light, we investigate the data quantity dependence of the hybrid models with limited data. In these experiments, we reduce the amount of training data and evaluate the hybrid models on the same test set (year 2021) as before. The MAPE results for these experiments, using limited training data, are displayed in Figure 14. The models are trained with a progressively decreasing number of months, ranging from January 15th to July 15th. The results for 12 months of training data are shown as a reference on the left side of the figure. For all experiments, we keep the same calibration of the EnergyPlus model as in the 12-months set-up, assuming ideal conditions.

Overall, we observe a decline in performance as the amount of training data decreases, with two notable exceptions at 3 months and 1 month. The 3-months performance is heavily influenced by the validation set, which predominantly consists of data collected in April. Since April has the highest indoor mean temperature and standard deviation, it does not serve as a representative validation set. This results in more biased models and poorer performance on the test set. The 1-month performance, however, is an evaluation artifact. Although the predictions cover less variance in the true room temperature, they are closer to the true temperature mean, resulting in a slightly better MAPE than when training with 2 months of data.

Among the models, the Residual-FFNN performs best, while the Surrogate-FFNN consistently shows the highest MAPE across all training data sizes. Additionally, the performance gap between the FFNN and Residual-FFNN widens as the amount of training data increases. Notably, from three months of training data, the limited data significantly impacts the FFNN's performance. In contrast, the Residual-FFNN effectively leverages the physical information from the EP simulation to generate more accurate predictions. An illustration of this can be seen in Figure 15, which shows predictions over the entire test set using only 1 month of training data. Similar effects can be observed in cases of LR and RF, depicted in Appendix Figure 19, Figure 20, Figure 21 and Figure 22. In summary, we see that the performance declines with decreasing training data while the residual approach maintains the best ability to cover the temperature variations.

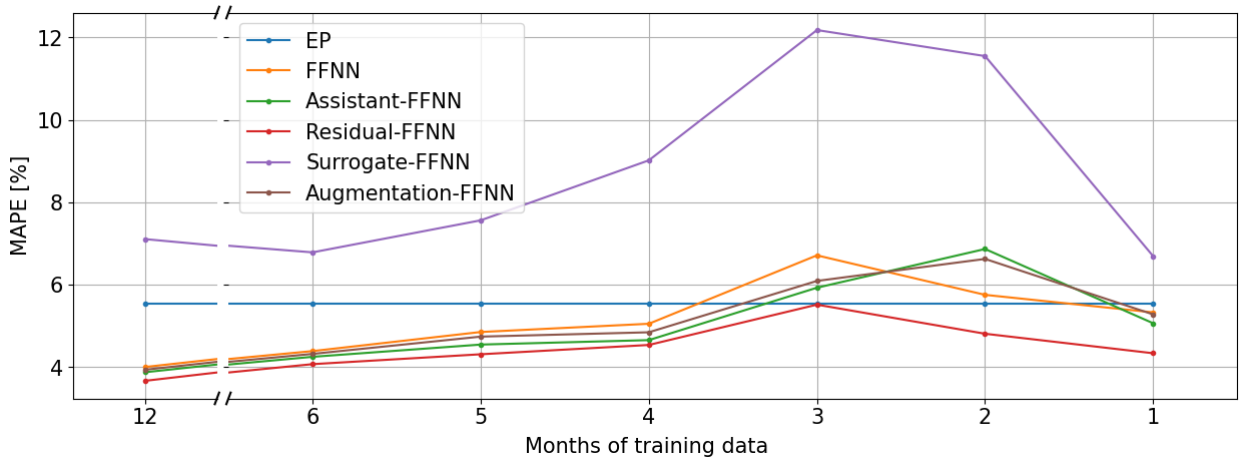


Figure 14: Average MAPE across all rooms for number of months of training data for all methods in the WBR-scenario.

5. Discussion

Our results indicate that more detailed documentation for the physics-based model and increased sensor availability significantly improve prediction accuracy. In scenarios with limited documentation and sensor data, hybrid approaches do not show substantial improvements over purely data-driven models. However, in scenarios with comprehensive documentation and abundant sensor data, hybrid methods demonstrate considerable performance enhancements. This suggests that hybrid approaches reach their full potential only when sufficient sensor measurements related to thermodynamics are available. Additionally, we observe that the most influential inputs vary depending on the hybrid approach used. For hybrid methods incorporating physics-based simulations as additional inputs (assistant and residual approaches), the feature group containing simulation data exhibits the highest relevance, indicating that the physics-based simulations provide the majority of information about thermodynamics. In contrast, for hybrid approaches like augmentation and surrogate, the importance is more evenly distributed across feature groups, indicating that these methods learn the dynamics directly from sensor data.

In scenarios with the highest documentation and sensor availability, different hybrid models perform best for different room types. However, the Residual-FFNN consistently achieves the best average performance across all rooms compared to the other hybrid models. We also find that the residual approach is most effective at capturing out of distribution behaviour, such as extended periods of window openings. Even in scenarios with limited data, the residual approach successfully captures temperature variations, whereas purely data-driven model and other hybrid approaches struggle. We attribute these advantages to the robust foundation provided by the physics-based model, combined with data-driven corrections. In stark contrast, the surrogate approach consistently performs the worst across all experiments, likely due to the physics-based model's performance setting an upper bound.

A limiting factor in the analysis of the limitations of training data is the assumption of ideal calibration of the physics-based model. With limited data available for calibration, the process may be suboptimal, leading to degraded performance of the physics-based model. We hypothesize that a residual-based approach could compensate for such systematic errors, whereas other hybrid approaches, such as surrogate models, may experience more significant performance limitations. Further studies are required to investigate the effects of calibration under these constrained conditions.

When applying the hierarchical Shapley value with the Residual-FFNN, we showcase the potential to detect biases in the physics-based component and identify areas for correction. Specifically, the feature importances in the residual approach show increased contributions to residual corrections at high outside temperatures, indicating that the physics-based model exhibits significant bias under these conditions.

For real-world deployment in control applications, the primary challenges are expected to include handling sensor faults, managing missing data, and adapting to usage behaviour changes due to shifting occupancy patterns. Compared to a purely physics-based model, the hybrid model is anticipated to have a minimal computational burden at inference. In selecting a suitable hybrid model, various criteria must be considered. The residual approach is best suited for



Figure 15: Predictions of FFNN and Residual-FFNN over the test set in the case of 1 month of training data.

compensating systematic biases in the physics-based model, such as deviations resulting from calibration errors or weather variability. The assisted approach similarly incorporates the physics-based simulation as feature, but its reliance on data-driven training means that the contribution of the physics-based simulation is determined by the model itself, offering practitioners less control. The surrogate model, in contrast, is primarily constrained by the performance of the underlying physics-based model making it less suitable for similar operation settings. The augmentation approach refines the surrogate model through fine-tuning on real data, potentially improving accuracy. However, finding an optimal tuning strategy can be complex and resource-intensive.

6. Conclusion

In this study, we assess the performance of four predominant hybrid approaches along with purely data-driven and physics-based models for predicting building temperatures. To mimic challenging real-world conditions, we evaluate these hybrid methods across three common scenarios that vary in documentation detail and sensor availability.

Furthermore, we explore the explainability of the hybrid approaches with the hierarchical Shapley value to account for feature dependencies. The results show that the residual approach is the most effective hybrid approach for temperature prediction, while the surrogate approach consistently exhibits the lowest accuracy. In terms of explainability, we showcased the adequacy of the hierarchical Shapley value to interpret the hybrid approaches. While the residual approach proved to be most effective in our settings, further improvements could involve weighting samples based on a certainty metric for correction. This would enable the residual model to prioritize time periods where higher error corrections are more significant. Future development of our study could involve conducting experiments on a larger scale, including a greater number of buildings and various building types beyond residential. In addition, while we considered multiple data scenarios, further investigation into data availability could involve more granular levels of building documentation. Another area for improvement is the assumption of ideal physics-based calibration when assessing the impact of limited training data on performance. We plan to address this by re-calibrating the physics-based model based on available data. An alternative research direction could explore an online setting for hybrid approaches, incorporating frequent re-calibration of the physics-based model as well as continuous re-training of the data-driven model.

CRedit authorship contribution statement

Leandro Von Krannichfeldt: Conceptualization, Methodology, Software, Investigation, Data curation, Writing - original draft, Writing - review & editing, Visualization. **Kristina Orehounig:** Supervision, Conceptualization, Writing - original draft, Writing - review & editing, Resources. **Olga Fink:** Supervision, Conceptualization, Writing - original draft, Writing - review & editing, Resources.

Data availability

The code and dataset are publicly available at the GitHub repository.

Acknowledgement

We thank all involved members from the Urban Energy Systems Laboratory at Empa and Intelligent Maintenance and Operations Systems Laboratory at EPFL. Special thanks go to Fazel Khayatian for insightful discussions about Building Energy Modeling and the nestli platform. This project is funded by Empa research & development grant 5213.00276.

References

- [1] International Energy Association, Buildings - Energy System (11 2023).
URL <https://www.iea.org/energy-system/buildings>
- [2] C. Deb, A. Schlueter, Review of data-driven energy modelling techniques for building retrofit, *Renewable and Sustainable Energy Reviews* 144 (2021) 110990. doi:<https://doi.org/10.1016/j.rser.2021.110990>.
URL <https://www.sciencedirect.com/science/article/pii/S1364032121002823>
- [3] P. Shen, W. Braham, Y. Yi, The feasibility and importance of considering climate change impacts in building retrofit analysis, *Applied Energy* 233-234 (2019) 254–270. doi:[10.1016/j.apenergy.2018.10.041](https://doi.org/10.1016/j.apenergy.2018.10.041).
URL <https://linkinghub.elsevier.com/retrieve/pii/S0306261918315976>
- [4] F. Khayatian, H. Cai, A. Bojarski, P. Heer, A. Bollinger, Benchmarking HVAC controller performance with a digital twin. doi:[10.46855/energy-proceedings-10382](https://doi.org/10.46855/energy-proceedings-10382).
URL <https://www.energy-proceedings.org/?p=10382>
- [5] U.S. Department of Energy, Energyplus™, version 00 (9 2017).
URL <https://www.osti.gov/servlets/purl/1395882>
- [6] S. M. Lundberg, S.-I. Lee, A unified approach to interpreting model predictions, in: I. Guyon, U. V. Luxburg, S. Bengio, H. Wallach, R. Fergus, S. Vishwanathan, R. Garnett (Eds.), *Advances in Neural Information Processing Systems* 30, Curran Associates, Inc., 2017, pp. 4765–4774.
URL <http://papers.nips.cc/paper/7062-a-unified-approach-to-interpreting-model-predictions.pdf>
- [7] Y. Pan, M. Zhu, Y. Lv, Y. Yang, Y. Liang, R. Yin, Y. Yang, X. Jia, X. Wang, F. Zeng, S. Huang, D. Hou, L. Xu, R. Yin, X. Yuan, Building energy simulation and its application for building performance optimization: A review of methods, tools, and case studies, *Advances in Applied Energy* 10 (2023) 100135. doi:[10.1016/j.adapen.2023.100135](https://doi.org/10.1016/j.adapen.2023.100135).
URL <https://linkinghub.elsevier.com/retrieve/pii/S2666792423000148>
- [8] G. Gokhale, B. Claessens, C. Devellder, Physics informed neural networks for control oriented thermal modeling of buildings, *Applied Energy* 314 (2022) 118852.

- [9] S. Nagarathinam, Y. S. Chati, M. P. Venkat, A. Vasan, PACMAN: physics-aware control MANager for HVAC, in: Proceedings of the 9th ACM International Conference on Systems for Energy-Efficient Buildings, Cities, and Transportation, BuildSys '22, Association for Computing Machinery, New York, NY, USA, 2022, pp. 11–20. doi:10.1145/3563357.3564052. URL <https://dl.acm.org/doi/10.1145/3563357.3564052>
- [10] Y. Chen, Q. Yang, Z. Chen, C. Yan, S. Zeng, M. Dai, Physics-informed neural networks for building thermal modeling and demand response control, *Building and Environment* 234 (2023) 110149. doi:10.1016/j.buildenv.2023.110149. URL <https://www.sciencedirect.com/science/article/pii/S0360132323001762>
- [11] J. Drgoña, A. R. Tuor, V. Chandan, D. L. Vrabie, Physics-constrained deep learning of multi-zone building thermal dynamics 243. doi:10.1016/j.enbuild.2021.110992. URL <https://www.sciencedirect.com/science/article/pii/S0378778821002760>
- [12] V. Taboga, C. Gehring, M. L. Cam, H. Dagdougui, P.-L. Bacon, Neural differential equations for temperature control in buildings under demand response programs, *Applied Energy* 368 (2024) 123433. doi:10.1016/j.apenergy.2024.123433. URL <https://www.sciencedirect.com/science/article/pii/S030626192400816X>
- [13] Z. Yang, A. D. Gaidhane, J. Drgoña, V. Chandan, M. M. Halappanavar, F. Liu, Y. Cao, Physics-constrained graph modeling for building thermal dynamics, *Energy and AI* 16 100346. doi:10.1016/j.egyai.2024.100346. URL <https://www.sciencedirect.com/science/article/pii/S2666546824000120>
- [14] L. Di Natale, B. Svetozarevic, P. Heer, C. N. Jones, Towards scalable physically consistent neural networks: An application to data-driven multi-zone thermal building models 340 121071. doi:10.1016/j.apenergy.2023.121071. URL <https://www.sciencedirect.com/science/article/pii/S030626192300435X>
- [15] X. Chen, T. Guo, M. Kriegel, P. Geyer, A hybrid-model forecasting framework for reducing the building energy performance gap, *Advanced Engineering Informatics* 52 101627. doi:10.1016/j.aei.2022.101627. URL <https://www.sciencedirect.com/science/article/pii/S1474034622000933>
- [16] R. E. Alden, E. S. Jones, S. B. Poore, H. Gong, A. Al Hadi, D. M. Ionel, Digital Twin for HVAC Load and Energy Storage based on a Hybrid ML Model with CTA-2045 Controls Capability, in: 2022 IEEE Energy Conversion Congress and Exposition (ECCE), 2022, pp. 1–5, iSSN: 2329-3748. doi:10.1109/ECCE50734.2022.9948141. URL <https://ieeexplore.ieee.org/document/9948141>
- [17] A. Verma, S. Prakash, A. Kumar, Ann-based energy consumption prediction model up to 2050 for a residential building: Towards sustainable decision making, *Environmental Progress & Sustainable Energy* 40 (3) (2021) e13544. doi:https://doi.org/10.1002/ep.13544. URL <https://aiche.onlinelibrary.wiley.com/doi/abs/10.1002/ep.13544>
- [18] F. Causone, S. Carlucci, M. Ferrando, A. Marchenko, S. Erba, A data-driven procedure to model occupancy and occupant-related electric load profiles in residential buildings for energy simulation, *Energy and Buildings* 202 (2019) 109342. doi:10.1016/j.enbuild.2019.109342. URL <https://www.sciencedirect.com/science/article/pii/S037877881930790X>
- [19] Y.-W. Lin, T. L. E. Tang, C. J. Spanos, Hybrid Approach for Digital Twins in the Built Environment, in: Proceedings of the Twelfth ACM International Conference on Future Energy Systems, e-Energy '21, Association for Computing Machinery, New York, NY, USA, 2021, pp. 450–457. doi:10.1145/3447555.3466585. URL <https://dl.acm.org/doi/10.1145/3447555.3466585>
- [20] R. Sterling, D. Coakley, T. Messervey, M. M. Keane, Improving whole building energy simulation with artificial neural networks and real performance data, in: Building Simulation and Optimisation Conference, 2014.
- [21] B. Cui, C. Fan, J. Munk, N. Mao, F. Xiao, J. Dong, T. Kuruganti, A hybrid building thermal modeling approach for predicting temperatures in typical, detached, two-story houses, *Applied Energy* 236 (2019) 101–116. doi:10.1016/j.apenergy.2018.11.077. URL <https://www.sciencedirect.com/science/article/pii/S0306261918317938>
- [22] B. Dong, Z. Li, S. M. M. Rahman, R. Vega, A hybrid model approach for forecasting future residential electricity consumption, *Energy and Buildings* 117 (2016) 341–351. doi:10.1016/j.enbuild.2015.09.033. URL <https://www.sciencedirect.com/science/article/pii/S0378778815302735>
- [23] F. Massa Gray, M. Schmidt, A hybrid approach to thermal building modelling using a combination of Gaussian processes and grey-box models, *Energy and Buildings* 165 (2018) 56–63. doi:10.1016/j.enbuild.2018.01.039. URL <https://www.sciencedirect.com/science/article/pii/S0378778817332942>
- [24] P. Westermann, M. Welzel, R. Evins, Using a deep temporal convolutional network as a building energy surrogate model that spans multiple climate zones, *Applied Energy* 278 (2020) 115563.
- [25] P. Westermann, R. Evins, Using Bayesian deep learning approaches for uncertainty-aware building energy surrogate models, *Energy and AI* 3 (2021) 100039. doi:10.1016/j.egyai.2020.100039. URL <https://www.sciencedirect.com/science/article/pii/S2666546820300392>
- [26] R. E. Edwards, J. New, L. E. Parker, B. Cui, J. Dong, Constructing large scale surrogate models from big data and artificial intelligence, *Applied Energy* 202 (2017) 685–699. doi:10.1016/j.apenergy.2017.05.155. URL <https://www.sciencedirect.com/science/article/pii/S0306261917307043>
- [27] R. K. Veiga, A. C. Veloso, A. P. Melo, R. Lamberts, Application of machine learning to estimate building energy use intensities, *Energy and Buildings* 249 (2021) 111219. doi:10.1016/j.enbuild.2021.111219. URL <https://www.sciencedirect.com/science/article/pii/S037877882100503X>
- [28] S. A. Sharif, A. Hammad, Developing surrogate ANN for selecting near-optimal building energy renovation methods considering energy consumption, LCC and LCA, *Journal of Building Engineering* 25 (2019) 100790. doi:10.1016/j.jobbe.2019.100790. URL <https://www.sciencedirect.com/science/article/pii/S2352710218311811>
- [29] A. Nutkiewicz, Z. Yang, R. K. Jain, Data-driven Urban Energy Simulation (DUE-S): A framework for integrating engineering simulation and machine learning methods in a multi-scale urban energy modeling workflow, *Applied Energy* 225 (2018) 1176–1189. doi:10.1016/j.

- apenergy.2018.05.023.
URL <https://www.sciencedirect.com/science/article/pii/S0306261918307165>
- [30] B. Choi, A. Nutkiewicz, R. Jain, Context-Aware Urban Energy Efficiency Optimization Using Hybrid Physical Models, in: *Climate Change AI, Climate Change AI*, 2020.
URL <https://www.climatechange.ai/papers/neurips2020/24>
- [31] Y. Ahn, B. S. Kim, Prediction of building power consumption using transfer learning-based reference building and simulation dataset, *Energy and Buildings* 258 (2022) 111717. doi:10.1016/j.enbuild.2021.111717.
URL <https://www.sciencedirect.com/science/article/pii/S037877882101001X>
- [32] S. A. Vaghefi, M. A. Jafari, J. Zhu, J. Brouwer, Y. Lu, A Hybrid Physics-Based and Data Driven Approach to Optimal Control of Building Cooling/Heating Systems, *IEEE Transactions on Automation Science and Engineering* 13 (2) (2016) 600–610. doi:10.1109/TASE.2014.2356337.
URL <https://ieeexplore.ieee.org/document/6913017>
- [33] F. Martellotta, U. Ayr, P. Stefanizzi, A. Sacchetti, G. Riganti, On the use of artificial neural networks to model household energy consumptions, *Energy Procedia* 126 (2017) 250–257. doi:10.1016/j.egypro.2017.08.149.
URL <https://www.sciencedirect.com/science/article/pii/S1876610217336354>
- [34] X. Chen, M. M. Singh, P. Geyer, Utilizing domain knowledge: Robust machine learning for building energy performance prediction with small, inconsistent datasets, *Knowledge-Based Systems* 294 (2024) 111774. doi:https://doi.org/10.1016/j.knosys.2024.111774.
URL <https://www.sciencedirect.com/science/article/pii/S095070512400409X>
- [35] M. Jain, K. Gupta, A. Sathanur, V. Chandan, M. M. Halappanavar, Transfer-learned models for predicting electricity consumption in buildings with limited and sparse field data, in: *2021 American Control Conference (ACC)*, 2021, pp. 2887–2894. doi:10.23919/ACC50511.2021.9483228.
- [36] A. Wohlfeil, CARNOT toolbox.
URL <https://ch.mathworks.com/matlabcentral/fileexchange/68890-carnot-toolbox>
- [37] Y. Liu, H. Chen, L. Zhang, Z. Feng, Enhancing building energy efficiency using a random forest model: A hybrid prediction approach, *Energy Reports* 7 (2021) 5003–5012. doi:https://doi.org/10.1016/j.egy.2021.07.135.
URL <https://www.sciencedirect.com/science/article/pii/S2352484721006016>
- [38] X. Chen, J. Abualdenien, M. M. Singh, A. Borrmann, P. Geyer, Introducing causal inference in the energy-efficient building design process, *Energy and Buildings* 277 (2022) 112583. doi:https://doi.org/10.1016/j.enbuild.2022.112583.
URL <https://www.sciencedirect.com/science/article/pii/S037877882200754X>
- [39] D. Wang, J. Landolt, G. Mavromatidis, K. Orehoung, J. Carmeliet, Cesar: A bottom-up building stock modelling tool for switzerland to address sustainable energy transformation strategies, *Energy and Buildings* 169 (2018) 9–26. doi:https://doi.org/10.1016/j.enbuild.2018.03.020.
URL <https://www.sciencedirect.com/science/article/pii/S0378778817337696>
- [40] K. Orehoung, L. Fierz, J. Allan, S. Eggimann, N. Vulic, A. Bojarski, CESAR-p: A dynamic urban building energy simulation tool 7 (78) 4261. doi:10.21105/joss.04261.
URL <https://joss.theoj.org/papers/10.21105/joss.04261>
- [41] C. M. Bishop, *Pattern Recognition and Machine Learning*, Information science and statistics, Springer.
- [42] R. Marcinkevičs, J. E. Vogt, Interpretable and explainable machine learning: A methods-centric overview with concrete examples, *WIREs Data Mining and Knowledge Discovery* 13 (3) (2023) e1493. doi:10.1002/widm.1493.
URL <https://wires.onlinelibrary.wiley.com/doi/10.1002/widm.1493>
- [43] L. S. Shapley, et al., A value for n-person games, *Annals of Mathematics Studies* (1953) 307–317.
- [44] G. Owen, Values of games with a priori unions, in: R. Henn, O. Moeschlin (Eds.), *Mathematical Economics and Game Theory*, Springer Berlin Heidelberg, Berlin, Heidelberg, 1977, pp. 76–88.
- [45] L. Rokach, O. Maimon, *Clustering Methods*, Springer US, Boston, MA, 2005, pp. 321–352.
- [46] M. H. Fulekar, *Bioinformatics*, Springer, 2009.
URL <https://link.springer.com/book/10.1007/978-1-4020-8880-3>
- [47] P. Richner, P. Heer, R. Largo, E. Marchesi, M. Zimmermann, NEST – una plataforma para acelerar la innovación en edificios, *Informes de la Construcción* 69 (548) (2018) 222. doi:10.3989/id.55380.
URL <http://informesdelaconstruccion.revistas.csic.es/index.php/informesdelaconstruccion/article/view/5879>
- [48] R. Mutschler, M. Rüdüsüli, P. Heer, S. Eggimann, Benchmarking cooling and heating energy demands considering climate change, population growth and cooling device uptake, *Applied Energy* 288 (2021) 116636. doi:10.1016/j.apenergy.2021.116636.
URL <https://linkinghub.elsevier.com/retrieve/pii/S0306261921001719>
- [49] F. Pedregosa, G. Varoquaux, A. Gramfort, V. Michel, B. Thirion, O. Grisel, M. Blondel, P. Prettenhofer, R. Weiss, V. Dubourg, J. Vanderplas, A. Passos, D. Cournapeau, M. Brucher, M. Perrot, E. Duchesnay, Scikit-learn: Machine learning in Python, *Journal of Machine Learning Research* 12 (2011) 2825–2830.
- [50] A. Paszke, S. Gross, S. Chintala, G. Chanan, E. Yang, Z. DeVito, Z. Lin, A. Desmaison, L. Antiga, A. Lerer, Automatic differentiation in pytorch (2017).
- [51] S. Hochreiter, J. Schmidhuber, Long Short-Term Memory, *Neural Computation* 9 (8) (1997) 1735–1780. doi:10.1162/neco.1997.9.8.1735.
URL <https://direct.mit.edu/neco/article/9/8/1735-1780/6109>

A. Additional results



Figure 16: Forecast visualization for a selection of hybrid models in the case of LR for bedroom 272 in the WBR-scenario. The predictions of the surrogate approach are omitted for better visibility. The grey shaded areas indicate the extended period of window openings.

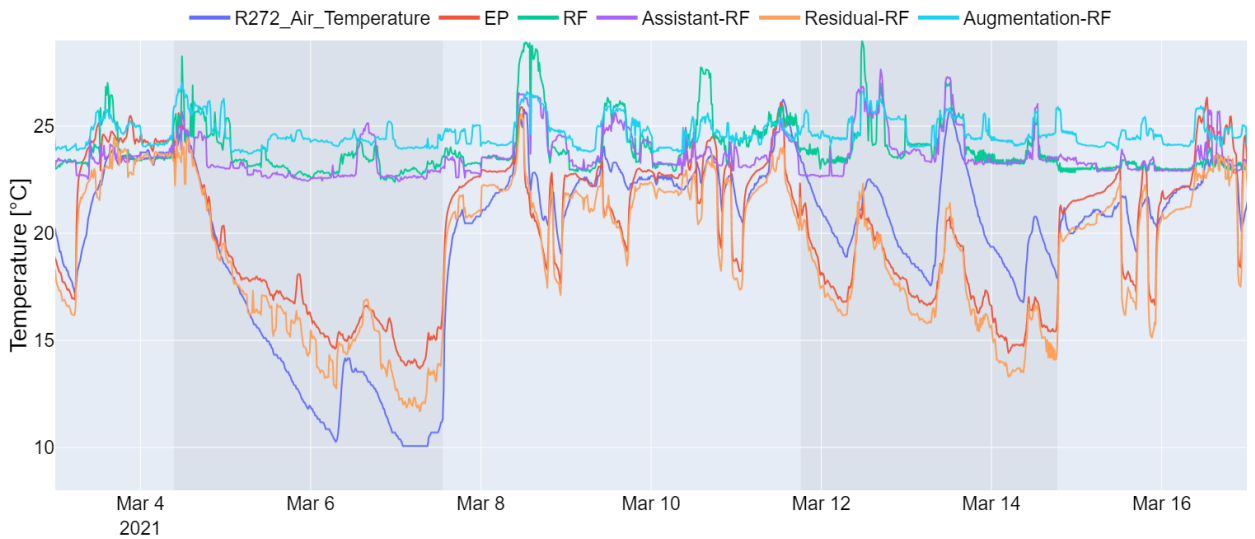


Figure 17: Forecast visualization for a selection of hybrid models in the case of RF for bedroom 272 in the WBR-scenario. The predictions of the surrogate approach are omitted for better visibility. The grey shaded areas indicate the extended period of window openings.

Method	MAPE [%]	MAE [°C]	RMSE [°C]
EP	5.54	1.25	1.59
LR	3.98	0.92	1.26
FFNN	4.00	0.92	1.26
RF	4.04	0.93	1.31
Assistant-LR	3.95	0.91	1.21
Assistant-FFNN	3.87	0.89	1.23
Assistant-RF	3.90	0.90	1.27
Residual-LR	3.95	0.91	1.21
Residual-FFNN	3.67	0.85	1.14
Residual-RF	3.82	0.89	1.21
Surrogate-LR	6.84	1.53	1.89
Surrogate-FFNN	7.11	1.59	1.94
Surrogate-RF	7.13	1.59	1.95
Augmentation-LR	4.07	0.94	1.27
Augmentation-FFNN	3.93	0.91	1.25
Augmentation-RF	5.72	1.28	1.62

Table 5: Average MAPE, MAE and RMSE across all rooms for each method in the WBR-scenario

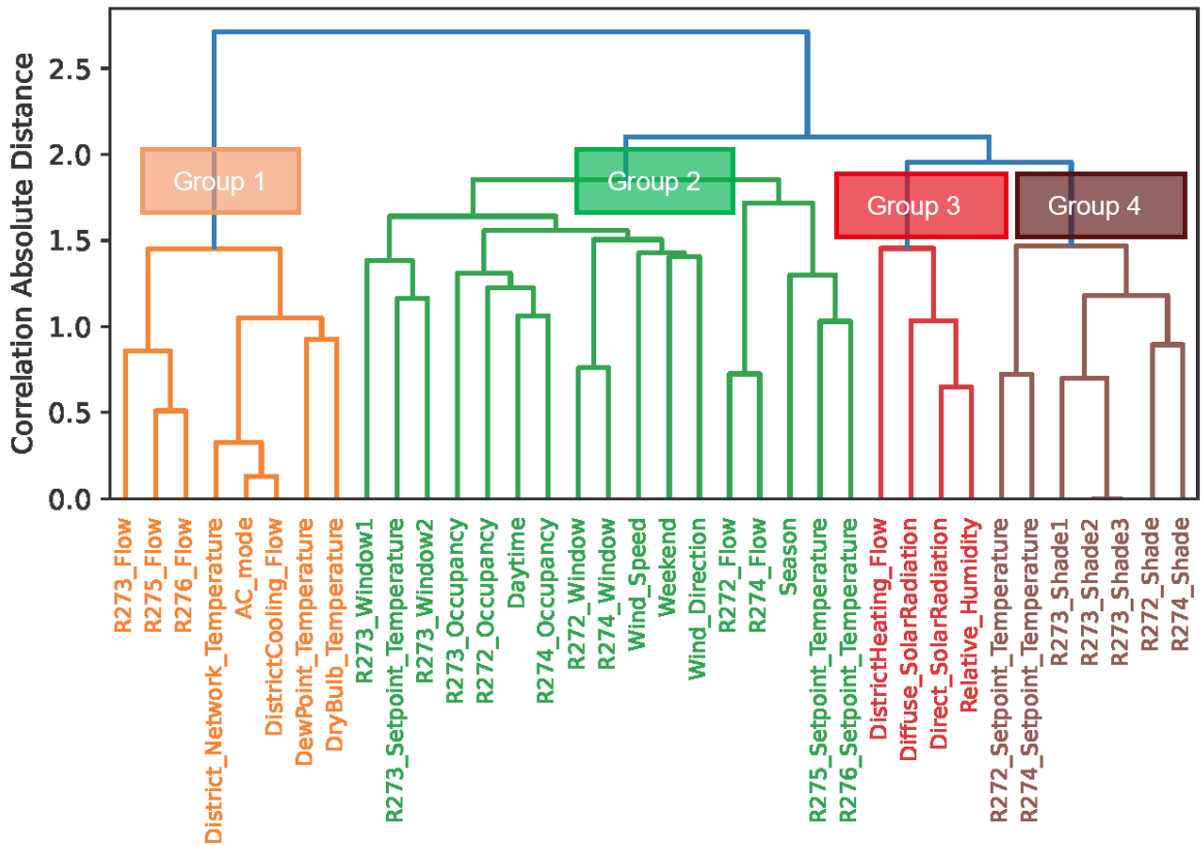


Figure 18: Dendrogram for input of data-driven, augmentation, and surrogate approach in the WBR-scenario.

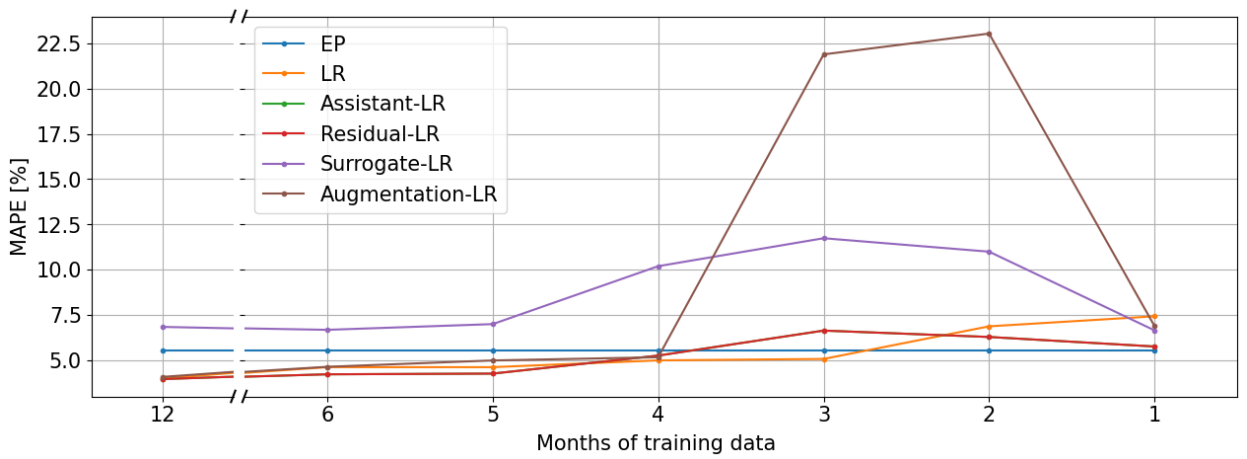


Figure 19: Average MAPE for LR across all rooms for number of months of training data for all methods in the WBR-scenario.

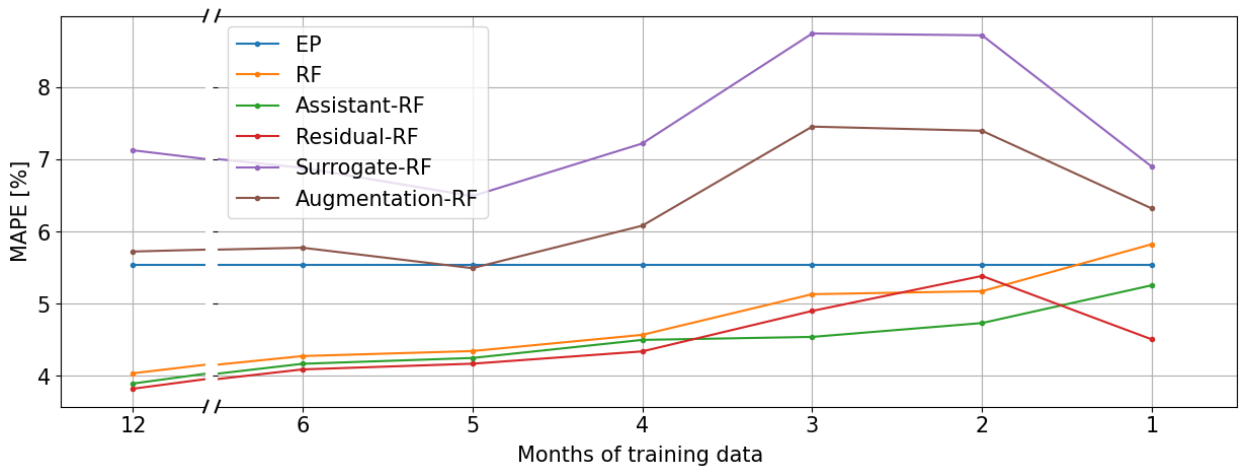


Figure 20: Average MAPE for RF across all rooms for number of months of training data for all methods in the WBR-scenario.



Figure 21: Predictions of LR and Residual-LR over the test set in the case of 1 month of training data.



Figure 22: Predictions of RF and Residual-RF over the test set in the case of 1 month of training data.

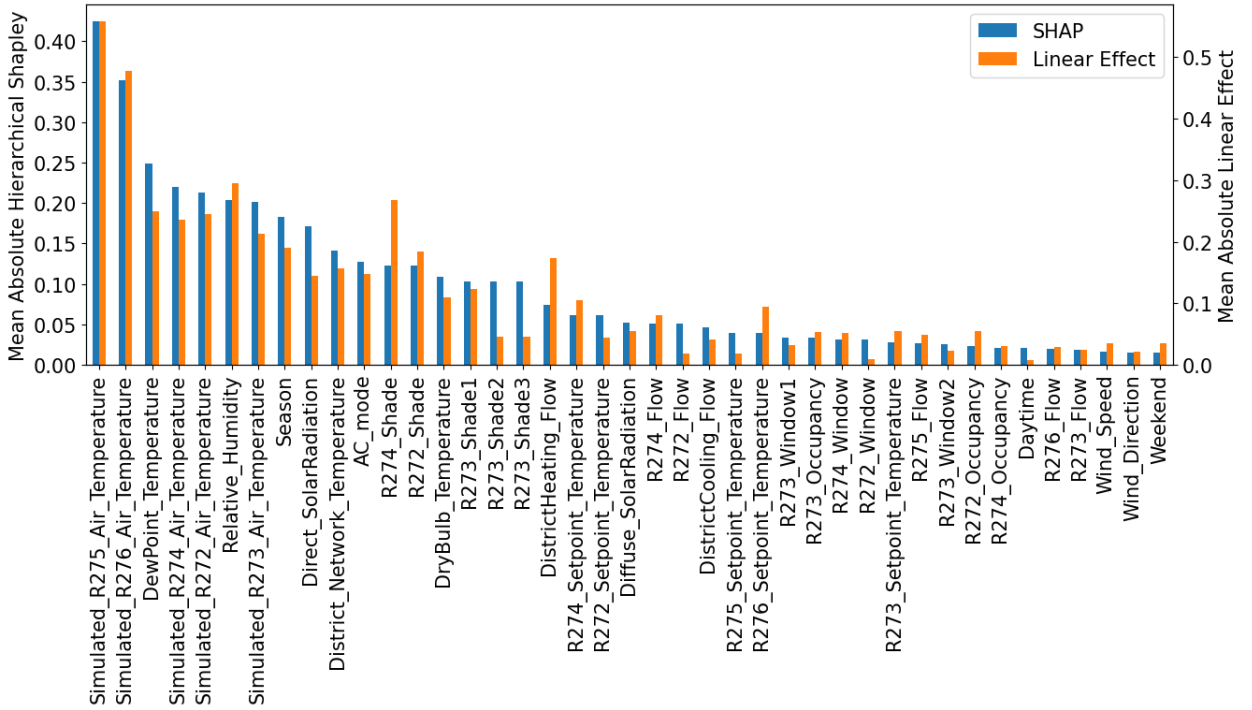


Figure 23: Bar plot of the mean absolute linear effects and hierarchical Shapley values for all features in the case of Residual-LR.

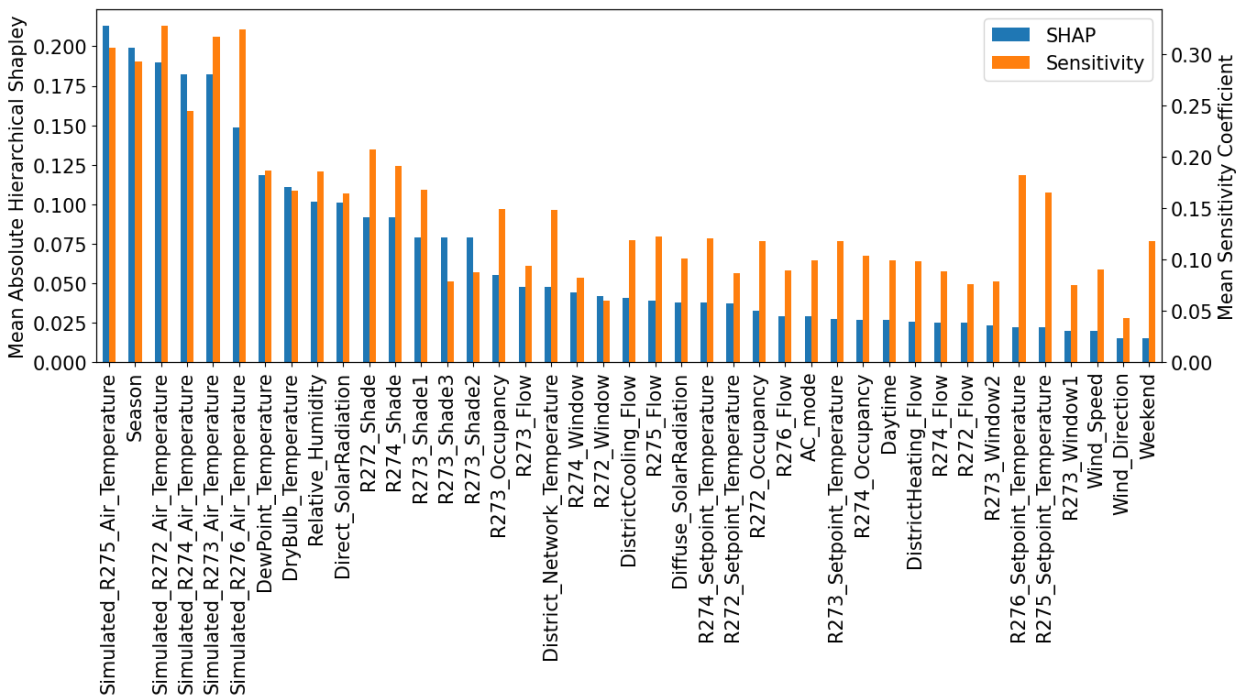


Figure 24: Bar plot of the mean absolute sensitivity coefficients and hierarchical Shapley values for all features in the case of Residual-FFNN.

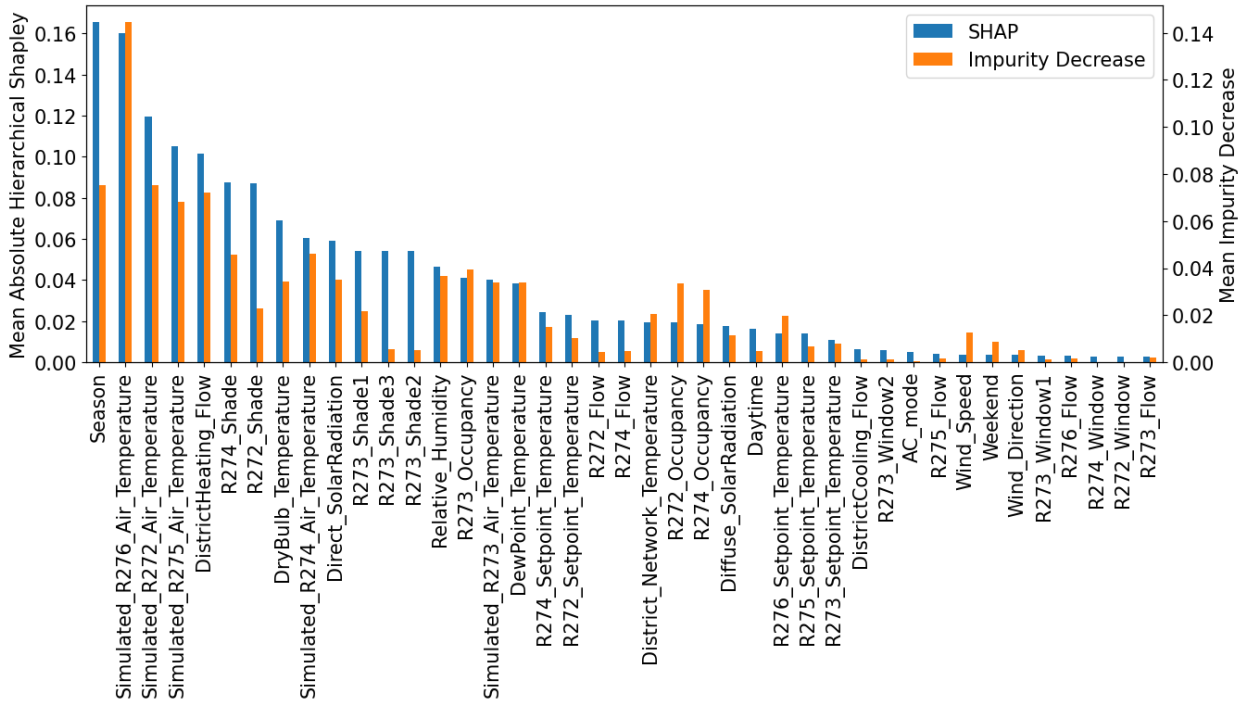


Figure 25: Bar plot of the mean impurity decrease and hierarchical Shapley values for all features in the case of Residual-RF.